LAPPEENRANTA-LAHTI UNIVERSITY OF TECHNOLOGY
LUT School of Energy Systems
LUT Mechanical Engineering

Juuso Viikilä

FINITE ELEMENT METHOD BASED REDUCTION OF WELDING DISTORTIONS IN WELDING OF A LOADER'S FRONT FRAME

Examiners: Professor Timo Björk
M. Sc. (Tech.) Antti Ahola

TIIVISTELMÄ

Lappeenranta-Lahti University of Technology
LUT School of Energy Systems
LUT Mechanical Engineering

Juuso Viikilä

Hitsausmuodonmuutosten vähentäminen lastaajan eturungon hitsauksessa elementtimenetelmän avulla

Diplomityö

2020

58 sivua, 26 kuvaa, 6 taulukkoa ja 20 liitettä

Tarkastajat: Professori Timo Björk
DI Antti Ahola

Hakusanat: Elementtianalyysi, hitsausmuodonmuutos, hitsaus, hitsausjärjestys

Tässä diplomityössä tutkitaan hitsausmuodonmuutoksia elementtianalyysin avulla. Hitsausmuodonmuutoksia pyritään vähentämään Sandvikin LH621-lastaajan eturungon hitsauksessa etsimällä uusia hitsausjärjestyksiä, joilla hitsausmuodonmuutokset olisivat pienemmät. Työssä tutustutaan hitsausmuodonmuutostyyppeihin, niiden syntymiseen sekä niiden ehkäisemiseen. Tässä työssä hitsausmuodonmuutoksiin pyritään vaikuttamaan juuri hitsausjärjestyksen avulla, mutta muitakin tapoja niiden ehkäisemiseksi on runsaasti.

Työn aloitusvaiheessa alkuperäinen hitsausjärjestys kirjattiin ylös hitsaustyön aikana ja runko mitattiin 3D-skannerin avulla kahdesti; silloitushitsauksen jälkeen ja kun runko oli hitsattu valmiiksi. Tällä varmistettiin, että analyysin tulokset ovat käyttö- ja vertailukelpoisia. Merkittävimmät muodonmuutokset syntyivät rungon kylkilevyihin. Tämän tiedon valossa käytettyä mallia voitiin yksinkertaistaa runsaasti, eikä rungon sisäosien hitsejä sisällytetty analyysiin ollenkaan.

Saatujen tulosten perusteella voidaan todeta, että kyseisessä rakenteessa hitsausmuodonmuutoksiin voidaan kyllä vaikuttaa muuttamalla hitsausjärjestystä, mutta kyseisessä rungossa niitä ei voida juurikaan pienentää alkuperäisestä suuruudestaan. Suurin syy tähän on hitsien epätasainen jakaantuminen kylkilevyjen ulko- ja sisäpuolella.

ABSTRACT

Lappeenranta-Lahti University of Technology
LUT School of Energy Systems
LUT Mechanical Engineering

Juuso Viikilä

Finite element method based reduction of welding distortions in welding of a loader's front frame

Master's thesis

2020

58 pages, 26 figures, 6 tables and 20 appendices

Examiners: Professor Timo Björk
M. Sc. (Tech.) Antti Ahola

Keywords: Finite Element Analysis, welding distortion, welding, welding sequence

Welding distortions are investigated in this research. They are tend to be reduced in welding of Sandvik's LH621 loader's front frame by finding new alternative welding sequences with the help of Finite Element Method. At first, distortion types are introduced as well as their establishing mechanism and ways to prevent them. In this research, distortions are tend to be reduced only with finding new alternative welding sequences although there are many other ways, too.

In the beginning of the work, the original welding sequence was registered during welding process. The examined frame was scanned with 3D-scanner twice; first after tack welding and secondly after welding work was done. With that, it was ensured that the results from the analysis were fit for use. The most significant distortions were formed to the side plates of the frame. Because of that, the model used in the analysis was simplified a lot; analysis was run only for a half of the frame's model and the welds at the interior of the frame were excluded.

Based on the analyses it can be concluded that one can have an influence on welding distortions in this structure by editing the welding sequence. However, they cannot be reduced below the level they were with the original welding sequence only with editing the welding sequence. The reason to this is that there are significantly more weld on the inner surface of the side plates than on the outer surface.

ACKNOWLEDGEMENTS

I would like to thank Sandvik Mining & Construction Oy for providing me this interesting topic for Master's thesis. I would like to thank my supervisor Tuomas Varpula from Sandvik for giving me instructions during this work. I also want to thank my other supervisor and the examiner of this thesis, Timo Björk. Special thanks goes to Reijo Lindgren whose advices for using the Abaqus software were irreplaceable. I want to say thanks for CSC IT Center for Science for providing the Abaqus software for this research.

Most of all, I would like to show my gratitude to my family for the support and encouragement during my studies. I also would like to say that I am grateful for all the friends I have had in my life throughout these years in Lappeenranta.

Juuso Viikilä
In Pori, 29th of June 2020

TABLE OF CONTENTS

SYMBOLI- JA LYHENNELUETTELO

α	Coefficient of heat expansion [1/ ° C]
ε	Strain [unitless]
η	Coefficient of process efficiency [unitless]
σ	Stress [MPa]
σ_{sb}	Stefan-Boltzmann's constant [5.67 x 10^{-8} W/m^2K^4]
σ_x	Normal stress component in X-direction
σ_y	Normal stress component in Y-direction
σ_z	Normal stress component in Z-direction
τ	Lag factor of double elliptical heat source
τ_{xy}	Shear stress component in XY-plane
τ_{yz}	Shear stress component in YZ-plane
τ_{zx}	Shear stress component in ZX-plane
ϵ	Emissivity [unitless]
c	Specific heat [J/kg ° C]
E	Young's modulus [GPa]
I	Welding current [A]
k	Thermal conductivity [W/m ° C]
q	Power density [W/m^3]
q_x	Heat flux [W/m^2]
R_{eL}	Yield stress [MPa]
Q	Heat input [kJ/mm]
U	Arc voltage [V]

AWI	Abaqus Welding Interface
CAE	Computer Aided Engineering
FEM	Finite Element Method
HAZ	Heat Affected Zone

1 INTRODUCTION

This master's thesis takes a look at reducing welding distortions and residual stresses in welding of front frame of a loader with the help of Finite Element Method (FEM). Focus of the research is on finding new alternative welding sequences, which are analyzed by FEM. The research is produced for Sandvik Mining & Construction Oy, which manufactures underground loaders and trucks for mining industry at their factory in Turku. This thesis involves one of the largest loaders that they manufacture at their plant of Turku. Object of the research, LH621 –loader is shown in figure 1.

Figure 1. LH621 –loader (Sandvik Mining & Rock Technology, 2018).

LH621 –loader was chosen to the research because its production volume was high at the time of the investigation and the welding deformations in its front frame were rather repetitive. The software used in research was Abaqus CAE/2017. Abaqus offers also Abaqus Welding Interface (AWI), which is a time-reducing plug-in for weld modeling. During this research, a new plug-in AWI Pro was also introduced, but it was not available for student licenses. It would have more versatile features for defining the heat source than original AWI has (double ellipsoidal heat source and possibility to give exact welding parameters as voltage, welding current and welding speed). The software was offered by CSC IT Center for Science, which offers student licenses for many software in engineering.

Necessary modifications such as creation of the grooves and welds to the 3D-model and deleting tiny and unnecessary details from the model was done in Solidworks 2017 before importing the model into Abaqus. Measurements of the tack welded and welded frames were done by 3D laser scanner, Creaform's Metrascan 3D.

1.1 Research problem

The research problem in this master's thesis is excessive welding distortions in the front frame of LH621 –loader. Especially there have been problems with side plates of the frame, which have been deformed by several millimeters. The distortions are harmful in assembling and they have also caused problems in machining. The welding deformations have sometimes been so significant, that the machining allowances have not been adequate. From the point of view of machining, one of the most important thing is that the reference surfaces of the side plates stay undeformed. They are used in co-operation with the surfaces of the side plates when setting the position of the frame in machining. Also, if the machined bushing line is not perpendicular with the centerline of the frame, the lifting arm which is mounted later can hit the other side plate instead of staying in the middle of the plates. The side plates of the frame need to be straightened with heat after welding because the upper edges of the plates are often bended inwards.

1.2 Research objective and defining the frames of the study

The target of the research is to find a welding sequence, which produces welding distortions in acceptable limits. Welding distortions are linked to machining allowance sufficiency, so the other target is to reduce problems in machining of the welded front frame. The alternative welding sequences are investigated with the help of Abaqus.

The front frame is mainly built from structural steel S355. Therefore, material properties and behavior during welding are presented mainly from this point of view. Welding parameters are excluded from the research although they have significant role in formation of welding distortions. Main reason to their excluding is that the number of time-consuming analyses would raise too high if they were included. Also, the alternative materials are excluded as well as phase deformations and viscoelastic behavior of the steel during welding.

2 BACKGROUND OF WELDING DISTORTIONS

It is possible that components to be welded already include residual stresses caused by previous manufacturing phases. For example, hot rolled products may cool down differentially at various regions of its structure. In this case the internal stress formulation is not regular throughout the cross section. Moreover, flanging, cutting or other forming processes may cause stresses and have an influence on the microstructure of the material nearby the formed area. Especially flame cut components have significant residual stresses. (Lepola and Ylikangas, 2016, p. 339)

Also welding causes irregular thermal stress to the working piece. The weld pool is small, point-shaped or elliptical hot spot and when it moves, it causes stresses in different directions. These stresses tend to change the shape of the welded component and create welding distortions. In welded structure, there are both residual stress and distortions. Residual stress causes problems with durability of the structure and welding distortions causes problems mostly in manufacturing. (Lepola and Ylikangas, 2016, p. 339)

Welding distortions have plenty of disadvantages. Rework is often required if the shape of the welded structure has changed. There can especially be need for straightening or machining of the components if high accuracy is demanded. Sometimes machining allowances have to be greater so that machining is still possible after welding deformations. Internal stress weakens the static durability and fatigue strength of the welded structure. It might induce buckling, collapsing, brittle fracture or assist stress corrosion later in use. Also the outlook of the product may suffer from the distortions. (Lepola and Ylikangas, 2016, p. 339)

2.1 Common types of welding distortions

Welding distortions are divided into two groups of deformation. First group retains welding deformations, which are consequence of longitudinal deformations. The second group retains welding deformations formed by cross-sectional deformations. (Lepola and Ylikangas, 2016, p. 339)

Longitudinal deformations include longitudinal shrinkage, bending and buckling. The group of cross-sectional deformations in turn contains transverse shrinkage, twisting and angular distortion. The grouping of welding distortions is presented in figure 2 including examples of each deformation type. (Lepola and Ylikangas, 2016, p. 339)

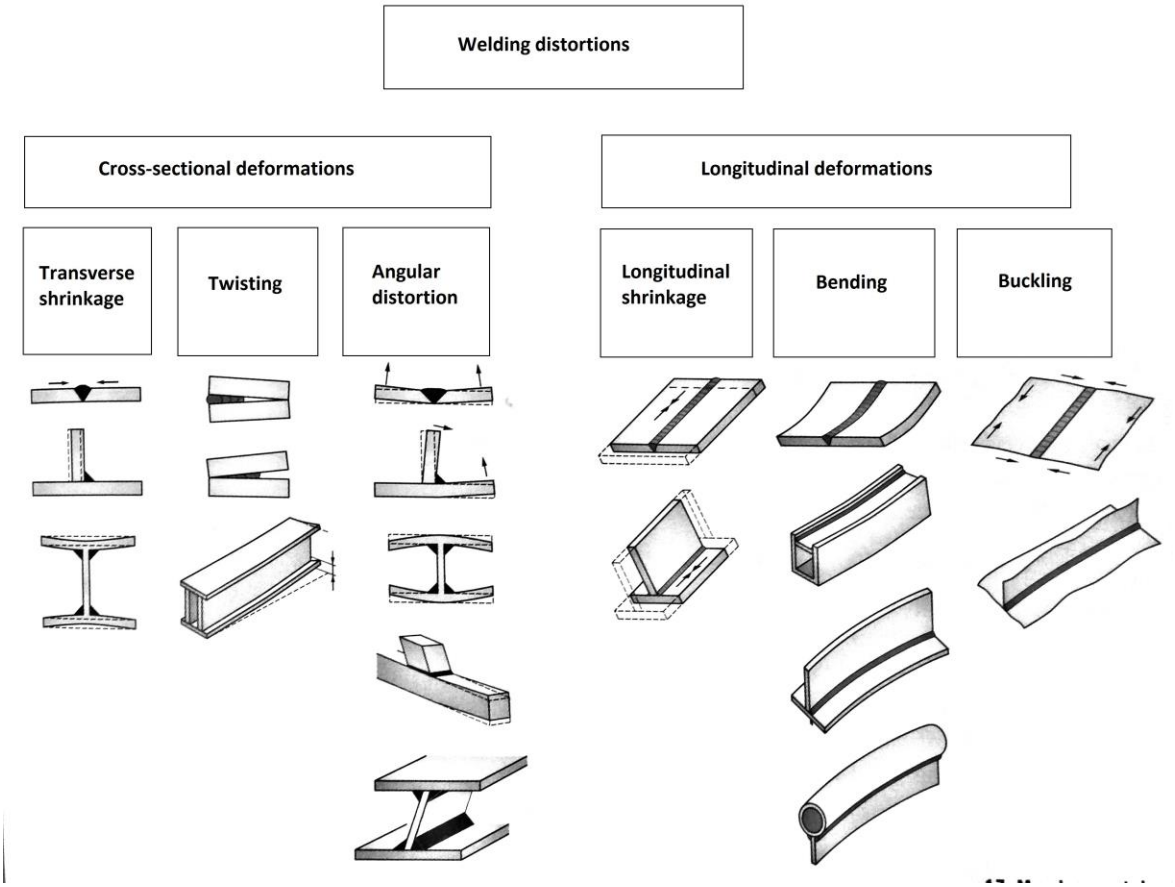

Figure 2. Common types of welding distortions (Lepola and Ylikangas, 2016, p. 339).

2.2 General stress state

General stress state can be defined with two main stress types: normal stress and shear stress. Stresses are always inspected in sectional planes. Normal stress appears perpendicular to the plane and shear stress appears parallel to it. General stress state in any situation can be described with three normal stress components (σ_x, σ_y and σ_z) and three shear stress components (τ_{xy}, τ_{yz} and τ_{zx}). Normal stress can be positive (tensile stress) or negative (compressive stress). The magnitude of normal stress σ can be defined as in equation 2:

$$\sigma = \frac{F}{A}, \tag{2}$$

where F is the force affecting perpendicular to cross-section of structure under inspection and A is the area of this cross-section. Depending on which components are active in each case, stress states can be divided into three categories. First category is axial stress state, where only one normal stress component is active. Second category is planar stress state. There can be one shear stress- and two normal stress components active, and they have to influence in the same plane; for example, they can be σ_x, σ_y and τ_{xy}. In the last category, the state of stress can be in any position in three-dimensional coordinate system. All six stress components can be active in the point of inspection. (Pennala, 2000, p. 15–18)

2.3 Strain

Under stress, the length of structure changes. This change is called strain ε, which is defined as follows:

$$\varepsilon = \frac{L - L_0}{L_0}, \tag{3}$$

where L_0 is the original length of the structure and L is the new length. Elastic strain can also be defined by stress σ and Young's modulus E, as seen in equation 4:

$$\varepsilon = \frac{\sigma}{E}. \tag{4}$$

In case of the most common structural materials, the strain grows elastically when the stress grows. Elasticity means that if the stress is removed, the length of the structure returns to its original length. This is not always the case. The strain can grow elastically only below yield point. If the stress grows higher than yield point, plastic deformation begins in the material. In this case, there appear both elastic and plastic strain. Even if the stress is removed the structure will not return to its original length, because plastic strain stays in material. Figure 3 shows the strain behavior depending on the elasticity or plasticity of the material. (Pennala, 2000, p. 19–25)

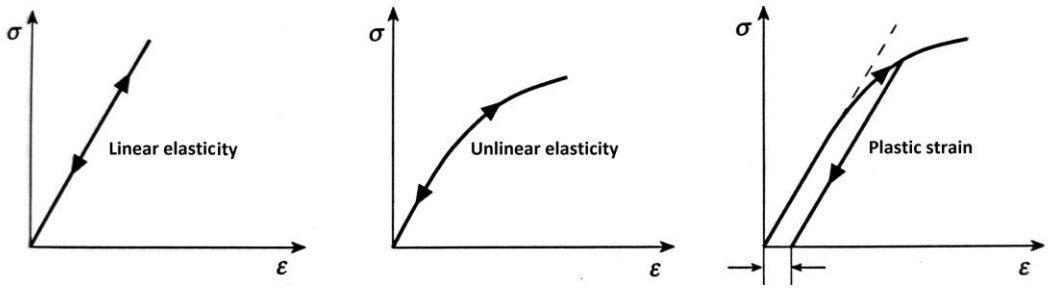

Figure 3. Connection between elasticity, stress value and strain. In the last figure, the stress has exceeded the yield point and permanent plastic strain is formed. (Pennala, 2000, p. 21)

2.4 Heat input

The energy of welding arc is partially absorbed into welded structure where it causes complicated heat transfer cycles. The energy of the arc is not completely absorbed into the structure because a part of it escapes via different heat losses. Absorbed amount of heat i.e. heat input Q (kJ/mm) can be calculated from equation 1:

$$Q = \eta \times \frac{I \times U}{v \times 1000}, \tag{1}$$

where η is a coefficient of thermal process efficiency, I is welding current as amperes, U welding voltage and v is traveling speed of the welding torch (mm/s). The coefficient of thermal process efficiency η can be considered as 0.8 in MAG welding. The equation exhibits that heat input increases if welding current and/or voltage increases and it decreases if travel speed of the torch increases. Heat input heats the material, which properties tend to vary with temperature. (Lukkari, 2007, p. 8; Keivani et al., 2014, p. 413)

2.5 Material properties at elevated temperatures

Mechanical and thermal properties of structural materials vary with temperature. The most important properties varying with temperature are Young's modulus E, yield stress R_{eL}, thermal expansion α, thermal conductivity k and specific heat c. The Young's modulus and yield stress of the structural steels clearly begin to decrease when the temperature rises above 300 °C. Decreasing is steady until the temperature is approximately 800 °C. After it, the decreasing is more gradual. Figure 4 illustrates the temperature dependency of Young's modulus and yield stress of steels. (Lawson and Newman, 1990, p. 7–8)

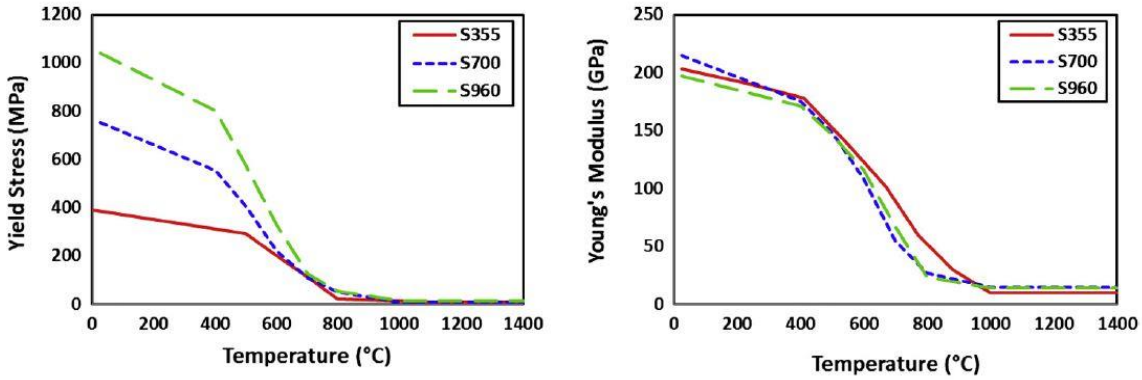

Figure 4. Temperature dependency of yield stress and Young's modulus (Bhatti et al., 2015, p. 882).

Thermal expansion is one of most important phenomenon in generation of welding distortions. In thermal expansion, the length of the structure variates when temperature changes. The change of the length Δl of a structure is defined as follows:

$$\Delta l = \alpha \times l \times \Delta T\,, \tag{5}$$

where α is coefficient of heat expansion, l is the original length and ΔT is the change of the temperature. (Lepola and Ylikangas, 2016, p. 340) Coefficient of thermal expansion of steel is slowly rising with temperature. At approximately 730 °C, the change is not as steady as at lower temperatures because phase transformations in the material affects the volume and density. (Lawson and Newman, 1990, p. 8)

The change of thermal conductivity by the temperature change is varying with different steels. For example, thermal conductivity of S355 is decreasing when temperature rises from room temperature to approximately 730 °C. In case of high strength steels, thermal conductivity can be lower at room temperature than at 730 °C. After that point, thermal conductivity begins to increase linearly again in case of all structural steels. Specific heat of steel rises slowly with the temperature. After approximately 720 °C, the phase transformations begin in the material. It consumes plenty of energy, which shows as a peak in the diagram of specific heat. Diagrams of these temperature dependent material properties of steel are presented in figure 5. (Bhatti et al., 2015, p. 880–882)

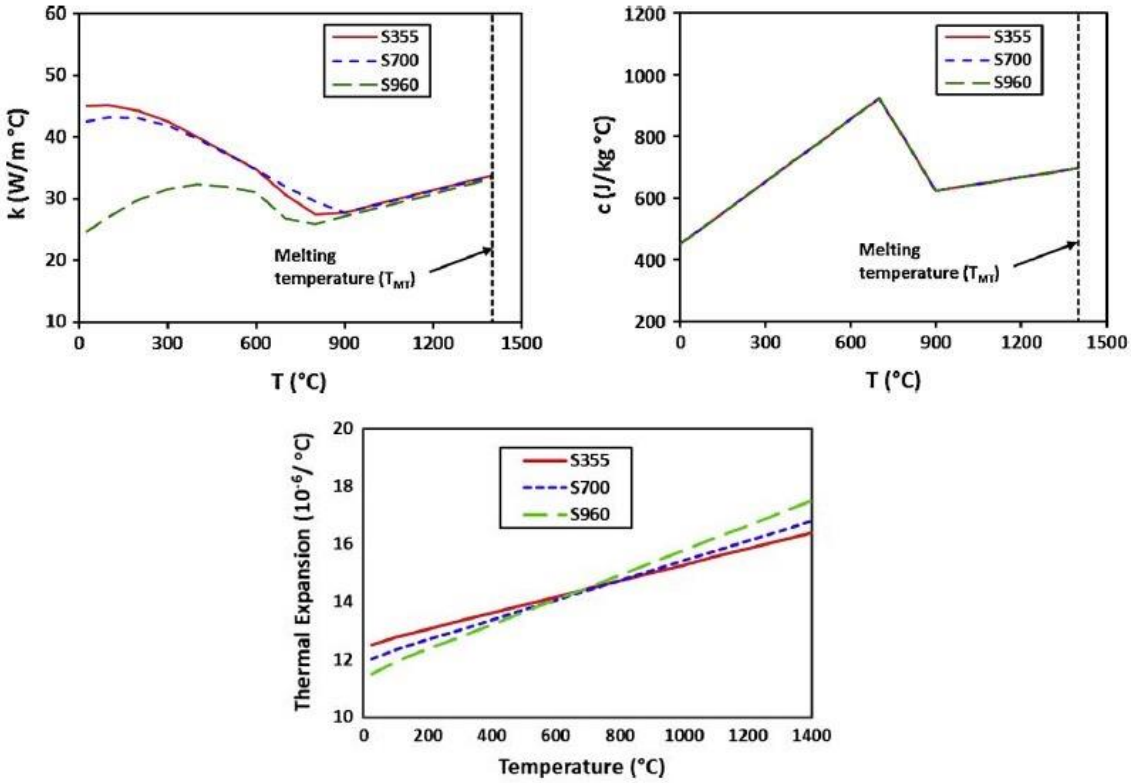

Figure 5. Temperature dependent heat conductivity, specific heat and thermal expansion of steel (Bhatti et al., 2015, p. 881, 882).

2.6 Establishing mechanism of welding distortions

The establishing mechanism of welding distortions is a multiphase chain of changes in the material properties. Welding changes thermal and mechanical material properties and microstructure, which are coupled together as seen in figure 6. (Goldak and Akhlangi, 2005, p. 9–10)

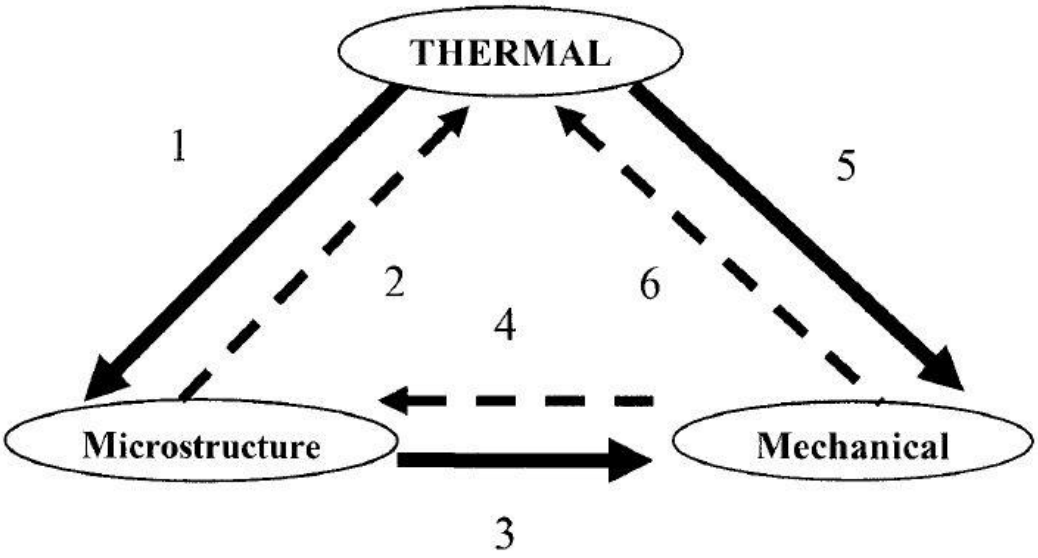

Figure 6. Coupling of thermal and mechanical material properties and microstructure (Goldak and Akhlangi, 2005, p. 10).

Explanation of the coupling in figure 6:

1. Microstructural changes in material appear at high temperatures.
2. Phase transformations have their latent heats. They act as heat sinks when the material is heating up and as heat sources when the material is cooling down.
3. Phase transformation changes the volume of the material. Moreover, every phase has different elastic and plastic properties.
4. Mechanical deformation and stress states in material affect to the new microstructure formation.
5. Thermal expansion affects linearly to the dimensions of the part and creates stresses.
6. Stress generates deformation and this deformation generates heat into the material. (Goldak and Akhlangi, 2005, p. 10)

Thermal expansion appears in material when the temperature rises. Moreover, the strength of the material begins to decrease so that when the temperature reaches approximately 1000 °C, the strength properties of the material are almost disappeared. In welding, the raise of the temperature is localized to a small area. This causes an irregular temperature field to the structure and thermal expansion is stronger in welded area and its neighborhood than further from it. The strength properties are greater in surrounding, colder material, which tends to

counteract the deformations caused by thermal expansion. Compression stress in the weld and its neighborhood upsets the material. (Lepola and Ylikangas, 2016, p. 340–341)

Once the weld starts to cool down, thermal contraction begins. Because the weld material and its neighborhood has upset, this area tends to contract into smaller dimension than it was before welding. Ambient, cooler material has still its strength properties greater than in weld and tends to prevent this shrinkage, too. Tensile stress forms in the weld and its neighborhood. (Lepola and Ylikangas, 2016, p. 340–341)

Tensile stress appears especially in the longitudinal direction of the weld, which can produce buckling especially with thin material thickness if fastening of the working piece is inadequate or geometry of the plate is unfavorable. Longitudinal tensile stress can lead into bending if the weld are located outside the neutral axis of the structure (The Welding Institute, 2011). Longitudinal tensile stress along the weld causes usually cross-sectional compression stress along the weld, but mostly at the ends of the weld. The magnitude of these stresses depends from the heat input, welding process and –position, plainness of the heat removal from the structure, quantity of weld beads, geometry of the groove and stiffness of the welded component. (Lepola and Ylikangas, 2016, p. 342)

The main types of cross-sectional welding distortions are angular distortion, transversal shrinkage and twisting. In angular distortion, there is stronger tensile stress near the top surface than in the middle and the bottom of the weld. This produces a differential stress profile throughout the cross-section of the weld bead, which tends to form angular distortion. The shape of the groove has its effect on angular distortion, too. With wedge-shaped grooves, the molten weld tends to shrink more at its surface, where the weld material is wider. Angular distortion is a common problem especially in multi-run-welded butt joints. In transverse shrinkage, shrinking weld is shortening the structure along the cross-section of the weld. Transverse shrinking can also move fillet welded plates compared each other yet their position stays invariant. In twisting, there appears “unequal longitudinal thermal expansion of the abutting edges” (The Welding Institute, 2011). (Lepola and Ylikangas, 2016, p. 342–343)

2.7 Prevention of welding distortions

Welding distortions can be prevented and controlled by many different ways. Planning of the structure, choosing the right welding process, planning the welding work and the working phases before welding are usual tools to prevent distortions. The most common procedures to prevent each distortion type are presented in table 1. (Lepola and Ylikangas, 2016, p. 343–344)

Table 1. Prevention procedure of welding distortions (Feng, 2005, p. 318–139; Lepola and Ylikangas, 2016, p. 343–344; The Welding Institute, 2011).

Distortion type	**Prevention procedures**
Transversal shrinkage	Reducing heat input, limiting the effective throat thickness in fillet welds, usage of clamps, groove choice; preferably X-shaped groove, two-sided welding, shortening of tack welds, step-back welding, narrowing the air gap, increasing the stiffness of the structure
Twisting	Reducing heat input, inserting all the tack welds before actual welding, increasing the number of tack welds, usage of clamps and supports
Angular distortion	Reducing heat input, limiting the effective throat thickness in fillet welds, limiting the number of weld beads, intermittent welding, pre-bending and positioning, pre-tensioning, usage of clamps
Longitudinal shrinkage	Reducing heat input, increasing the number of weld beads, intermittent welding, reduction the amount of tack welds and setting their welding direction from the edges towards the center of the weld, inserting the weld as close to the neutral axis of the structure as possible, changing welding sequence
Bending	Reducing heat input, setting the welds equally to the neutral axis of the structure
Buckling	Reducing heat input, pre-tensioning the structure with heat, usage of clamps and increasing the stiffness of the structure

2.8 Measured welding distortions in the frame with the original welding sequence

Welding distortions were measured with Creaform's MetraScan 3D-laser scanner. With it, it's possible to measure objects which volume is max. 16.6 m^3, so it is adequate to this target. Measuring accuracy is adjustable but can reach resolution of 0.122 mm. (Creaform, 2018) Measuring of welding distortion is divided into three phases:

1. Scanning tack welded frame
2. Scanning finish welded frame
3. Comparing the results from previous phases

The results of measurements were loaded into PolyWorks sofware for comparison. The result of a laser scanning consists from a vast number of measured points and looks like a 3D model of the frame. These points from both measurements are set one on the other and the difference between measurements (welding distortions) are illustrated by color mapping as seen in figure 7. User can also pick any point from the model, and the difference between measurements in that point is shown in millimeters in its own box.

One can see from the picture 7 that the most significant distortions have formed into the side plates of the frame. The largest difference between tack welded and finish welded frame is about 6 millimeters. The distortion values are represented as resultant vectors so they do not tell the direction of the welding distortion. However, it was ensured that most of the distortions formed parallel to side plate's normal and this resultant vector represents distortions in that direction well enough. Both side plates tend to pull inwards during welding. The coordinates of the analyzed model were set so that this direction is y-direction. Grey areas in the picture represent areas of the frame, which were measured only in the other scanning so they have no data to be compared. The schedule of scanning the tack welded frame was a bit tight and that's why the left side (upper picture) is defectively measured.

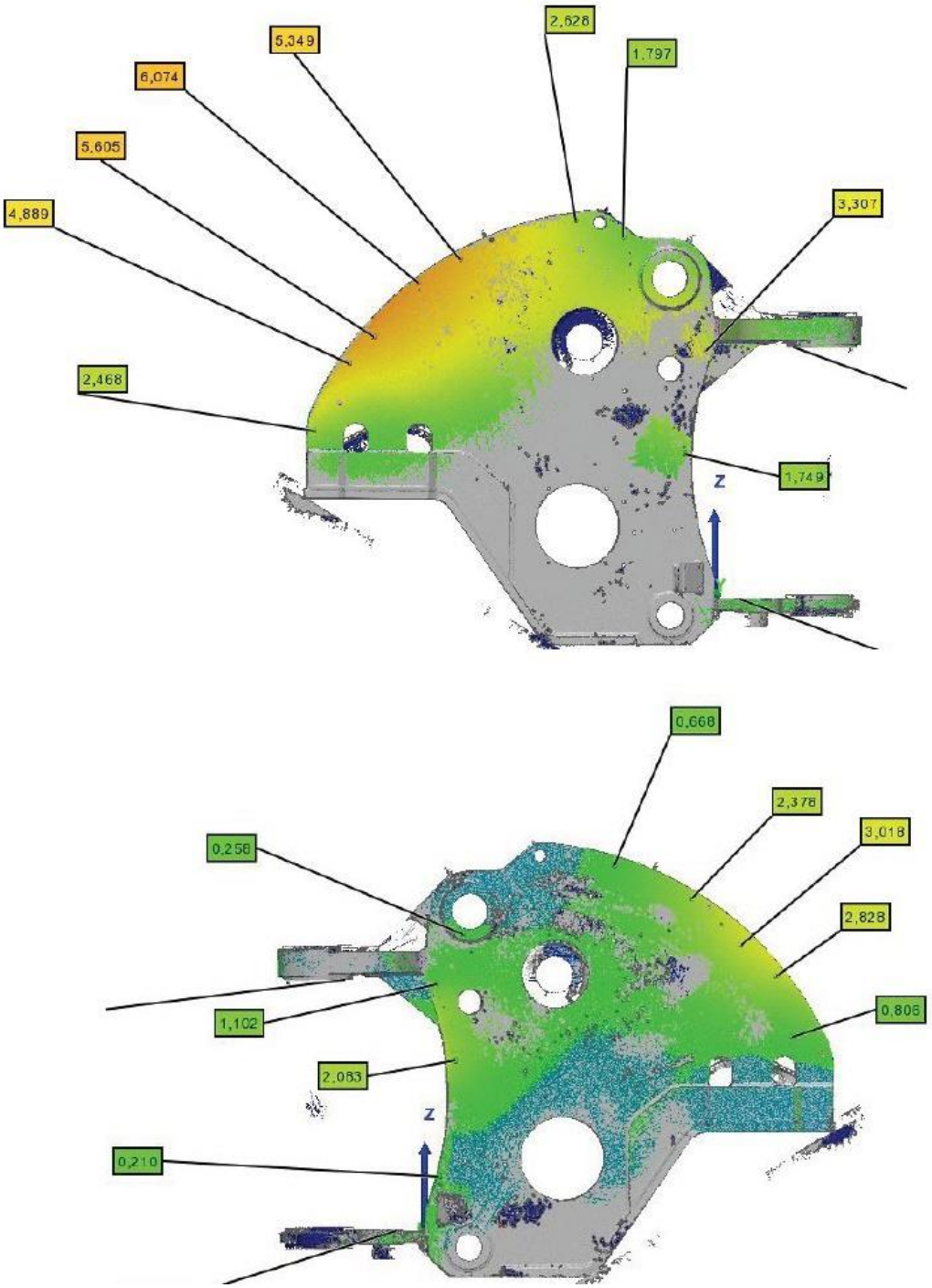

Figure 7. Measured welding distortions along the frame (all dimensions in mm).

3 ANALYSIS OF WELDING DEFORMATIONS BY FEM

This chapter introduces details, which are important to know about welding analyses in Computer Aided Engineering (CAE) -software. Different FEMs for predicting deformations are discussed first. After it, focus moves onto weld modelling by different methods of element activation, from there to heat source modelling and heat removal from the part, meshing of the part, constraints of the computational model and in the end, the analyzed cases with alternative welding sequences are introduced. In this chapter, it's also took an insight to methods that were not used in the analysis of this work but are considerable alternative ways to execute analysis in similar cases.

3.1 Thermal elastic-plastic method and inherent strain method

Predicting welding deformations can be divided into three main categories: experimental formulas, thermal elastic-plastic finite element method and inherent strain finite element method. Experimental formulas are usable only for rather simple structures and weldments, so they are not investigated in this research. Welding distortions are always a result of nonlinear behavior of the base material and weld material. However, in some cases the analysis can be executed as linear analysis to save computing time. (Jun-mei et al., 2005; Pillinger, 1992, p. 225)

3.1.1 Thermal elastic-plastic method

Thermal elastic-plastic FEM is an accurate method for predicting distortions and residual stress. It simulates welding process itself and physical phenomenon occurred during it. If large deformations are not expectable, material properties can be assumed to be linear during every small step of analysis. This method is very time consuming and it's usual that some simplifications are used in this method. However, the most accurate results are reached when no simplifications are used and the heat source is simulated to move along the weld as in real welding process. (Kim, Kang and Chung, 2015)

This method is used in this work due to its accuracy in complex structures although it's known that analysis will take remarkable amount of computing time. To reduce computing time, some of the material properties are described constant instead of nonlinear properties.

3.1.2 Inherent strain method

Inherent strain method approaches deformations from the point of view of internal strains, according to its name. The method is developed to an efficient method to calculate the welding distortions even in case of complex structures, but it's not as accurate as elastic-plastic method. Efficiency of this method compared to elastic-plastic method is based on usage of linear analysis instead of nonlinearity. Inherent strain method has plenty of applications adapted to different objects. (Deng, Murakawa and Ma, 2012; Park et al., 2014; Lee, Seo and Chung, 2018)

In this method, inherent strains are divided into two categories: ineffective strains and effective strains. The method is interested in these effective strains, which induce residual stress and deformation. Deformations can be calculated from these strains. Murakawa, Luo and Koide have expressed equations, which are used to solve the deformations during analysis. (Park et al., 2014; Murakawa, Luo and Koide, 1998, p. 61–65)

3.2 Simplifications and structural editions in 3D -model

Almost all of the editions of 3D-model of the front frame were done in Solidworks 2017 Education Edition. The original model didn't include neither welds or weld grooves so they were added to the original model. Convex shapes of the weld reinforcements were simplified to planar surfaces in order to keep the geometry as simple as possible so that meshing of the part in Abaqus was easier and didn't demand unreasonable amount of elements. For the same reason, all the tiny air gaps between parts of the frame's model, were removed. Also, small holes in the frame's plates were filled. Tiny details increase the mesh density locally, which is not desirable. There are few subassemblies in the frame, which components are already welded before finish welding. Each of these subassemblies were joined into one solid part in the model.

When those phases mentioned above, were completed, the model was imported into Abaqus, where welds were splitted into beads. Splitting was done in Abaqus due to its user-friendlier tool for partitioning. Simplified model of the whole front frame is shown in figure 8.

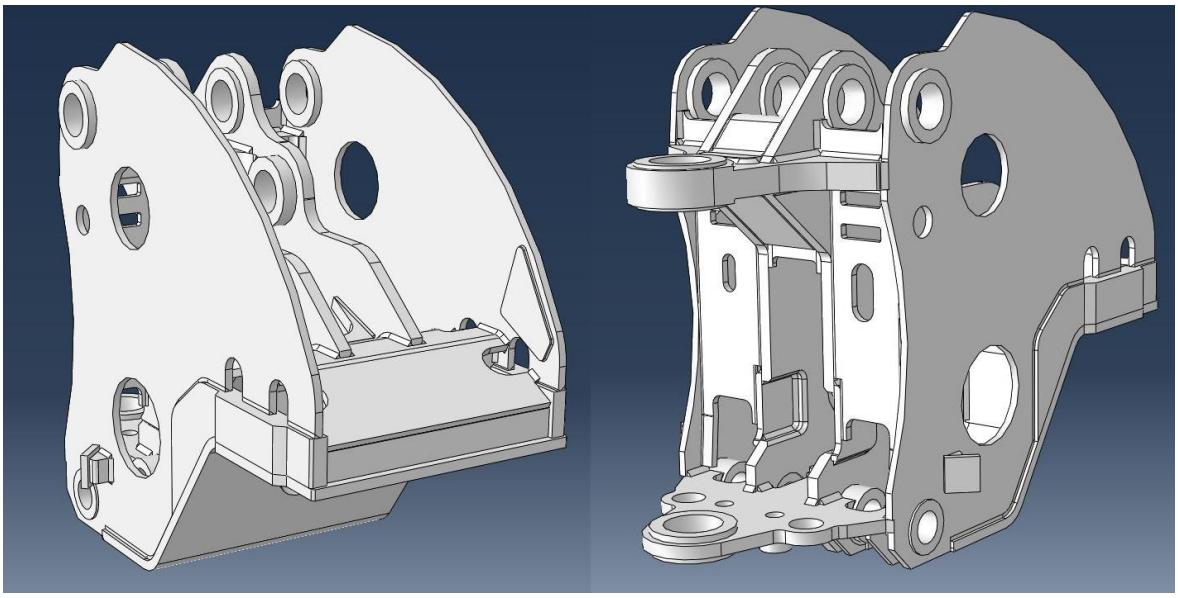

Figure 8. Simplified model of the front frame.

It was noticed, that most of the welding distortions appear in the side plates, so only welds having a contact with side plates were included to the analysis. Another important simplification was that the model was splitted into two halves due to its symmetry. It was determined that both sides should be welded symmetrically so this simplification doesn't make significant inaccuracy to the analyses. With this, it was possible to reduce computing time of each analysis by 50 %. The cutting plane was locked completely in y-direction (normal to the cutting plane) in analyses. It was estimated that the stiffness of the frame is so high that this boundary condition represents well enough the other side of the model and hence doesn't make the analysis inaccurate.

Original welding sequence was not equal in both side plates, so two analyses were executed from the original sequence, one for both sides. Modified welding sequences determined to be equal in both side plates, so only one analysis was necessary when they were analyzed. The two sides of the model are shown in figure 9.

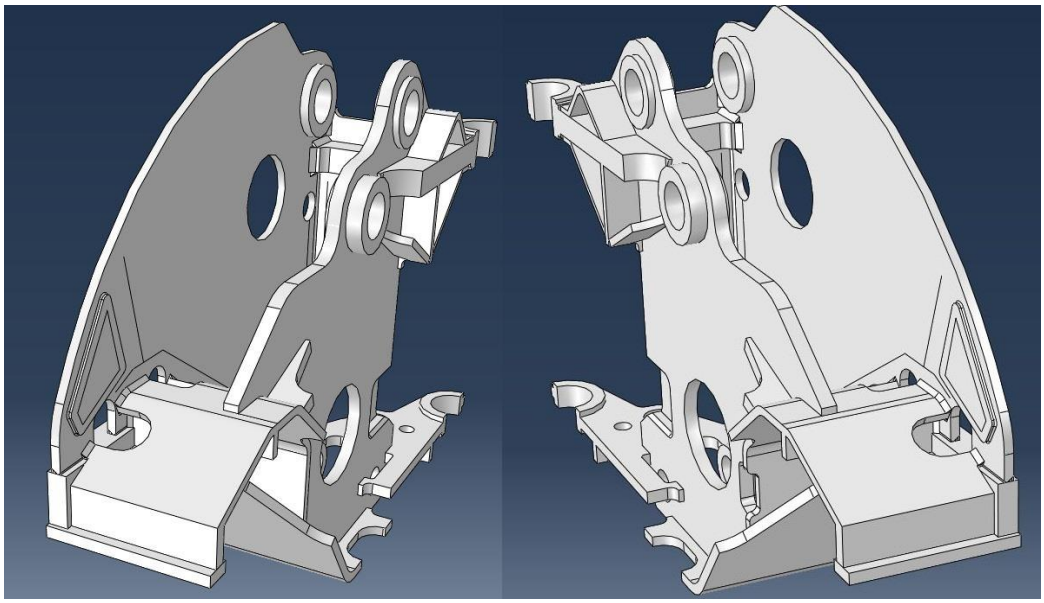

Figure 9. Splitted sides of the model.

3.3 Weld modelling

The geometry of the structure alternates continuously during welding because filler material is added into the grooves. Weld affects in stiffness of the structure and the heat convection in the base material near the weld. This inserting of the weld material must be noticed in order to produce realistic and reliable welding analysis. Casually there is two methods for laying weld beads down during welding analysis, silent element method and inactive element method. (Lindgren and Hedblom, 2001, p. 647–649)

3.3.1 Silent element method

In this method, the elements in every weld, also in the welds, which are not laid down yet, are included and active in the model almost all the time from the beginning of the analysis until its end. The material properties of those elements mentioned last, are made as passive as possible to avoid their effect to the rest of the model. Main ways to make them passive are to decrease their heat conductivity and stiffness. Nevertheless, these properties shouldn't be given a value too low, because it may produce invalid matrix of stiffness. It may require a few test simulations to find appropriate values. (Lindgren, Runnemalm and Näsström, 1999, p. 1308)

When a weld bead is laid down, the corresponding elements including strain and stress are first deleted from the model and then reinserted strain-freely with normal material properties.

This is done with quick model change step between weld passes. This method has two advantages. First one is that the passive elements of the welds move and adapt with the structure during earlier weld passes so that their shape and dimensions are suitable when inserted to the model. Second advantage is the suitability of this method to most of the CAEs. (Lindgren, Runnemalm and Näsström, 1999, p. 1308–1309)

3.3.2 Inactive element method

In inactive element method, the elements of the welds are created during simulation step by step. In the beginning, all of the weld beads and their elements are deleted from the computational model. Corresponding elements of each weld bead are then created again and reinserted into the model strain-freely within the weld pass in which the bead is laid down. The locations and positions of all weld elements are defined on the original geometry of the structure but the geometry deforms during every weld pass. This is why the data of the geometry requires restructuring after every weld pass. The elements, which are not created yet, are inactive and don't deform with earlier welding deformations. This may lead into inaccurate results if the deformation is significant, because the dimensions of the elements are distorted when inserted into the model. (Lindgren, Runnemalm and Näsström, 1999, p. 1309)

Silent element method and inactive element method are both functioning methods for modelling welds in finite element analysis. Lindgren, Runnemalm and Näsström have distinguished that both approaches can give very similar results. However, due to their research it seems that inactive element method may produce more accurate results and computing time is reduced by 5 % compared to silent element method. (Lindgren, Runnemalm and Näsström, 1999, p. 1314) Inactive element method was used in this work because it seemed to produce more accurate results in analysis of a test welded part. Test welding and model calibration are discussed more in chapter 3.9.

3.4 Heat transfer in welds

To get accurate results in simulation of welding distortions, it is necessary to know the heat cycle in the material during welding. Most important parts of the heat cycle, from the point of view of welding distortions, are holding time in high temperatures and cooling time between 800 °C and 500 °C. The microstructure in the weld and heat affected zone (HAZ) are determined during this cooling interval. Another important cooling interval is between 400

°C and 150 °C. This interval has its effect on hydrogen diffusion and cold cracking, but this is not discussed more in this work, because the focus is on distortions. (Goldak, Chakravarti and Bibby, 1984, p. 299)

3.4.1 Heat source modelling

Many alternative options have been tested for modeling the heat source of arc welding. First suggestions were point-shaped and line-shaped, but the infinity of power density became a problem with them. Goldak, Chakvarati and Bibby introduced a double ellipsoidal heat source model in 1983, which is commonly used and accurate option for modelling heat source in arc welding. The picture of it is shown in figure 10. (Goldak and Akhlangi, 2005, p. 22–32; Goldak, Chakravarti and Bibby, 1984, p. 299–300)

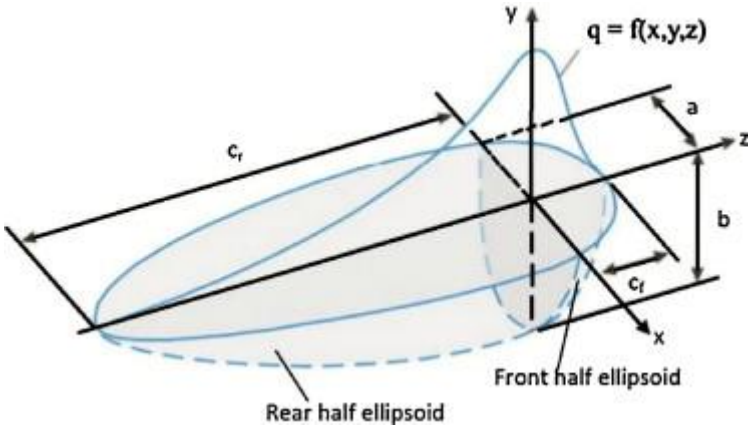

Figure 10. Double ellipsoidal heat source model (Jia et al., 2014).

To calculate the power density q at the time t in front quadrants of this model, one can use equation 6:

$$q(x,y,z,t) = \frac{6\sqrt{3}f_f Q}{abc\pi\sqrt{\pi}} e^{-3x^2/a^2} e^{-3y^2/b^2} e^{-3[z+v(\tau-t)]^2/c^2}. \quad (6)$$

Respectively, the power density in rear quadrants is defined as follows:

$$q(x,y,z,t) = \frac{6\sqrt{3}f_r Q}{abc\pi\sqrt{\pi}} e^{-3x^2/a^2} e^{-3y^2/b^2} e^{-3[z+v(\tau-t)]^2/c^2}. \quad (7)$$

In equations 6 and 7, Q is energy input rate from the arc, a, b and c are width, depth and length of the front and rear quadrants. In turn, v is the speed of the heat source i.e. welding speed and τ is a lag factor, which defines the position of the heat source in the beginning. Fractions f_f and f_r are used to define the power distribution between front and rear quadrants of the heat source model. Because the power distribution is supposed to be continuous throughout the model, these fractions need to fulfill the equation 8. (Goldak and Akhlangi, 2005, p. 28–32)

$$f_f + f_r = 2. \tag{8}$$

Moving, realistic double elliptical heat source produces the most accurate simulation results, but its disadvantage is poor computing efficiency. With large models, using this heat source model may be unnecessarily time-consuming. If computing time needs to be reduced, some simplifications may be considerable. Common way to simplify the heat source is to bring the heat to whole weld bead at the time. (Pu et al., 2017, p. 2215–2216)

Instantaneous heat source model can achieve high accuracy in prediction of residual stress. However, accuracy in prediction of welding distortions is not as good as when moving heat source is used. Despite this, instantaneous heat source model is used in this work, because it is shown, that it can save approximately 50 % computing time compared to moving heat source when the same mesh density was used. (Pu et al., 2017, p. 2225) When instantaneous heat source is used in Abaqus, the heat source is simulated by adding prescribed temperature into elements corresponding to weld bead laid down. The heat input can be adjusted by changing the length of heating period and if wanted, by changing the holding time at the highest temperature. (Dassault Systèmes SIMULIA Corporation Inc., 2014, p. 5)

3.4.2 Heat flux inside the structure and heat removal from the structure

If arbitrary point of a metallic part is heated, temperature all over its volume begins to rise. Temperature rises more quickly near the heat source. This heat conduction is based on vibration and collisions of neighboring molecules in the structure. Molecular activity is greater at the point of heat source, and chain reaction of molecules establish heat flow towards cooler areas in the part. Naturally, heat flow goes always from higher temperature to lower. That means also, that if the temperature is higher inside the structure than on its surface, the heat

flux is towards its surface. Heat flux q_x can be calculated from Fourier's law, which is presented in equation 9: (Jiji, 2006, p. 3–4)

$$q_x = -kA\frac{dT}{dx}. \quad (9)$$

In this equation, *k* is thermal conductivity of the material, i.e. film coefficient, *A* is the area through which the flux flows, *dT* is the temperature difference over the heat flux and *dx* is the distance over the heat flux calculated. (Jiji, 2006, p. 3–4)

The heat escapes by radiation from structure's surfaces. The energy of radiation depends on geometry of the structure, area of the surfaces, emissivity of the surfaces and absorptivity of surrounding surfaces. The calculation of heat exchange between two surfaces is often complex because the absorptivity of surrounding surface is only a fraction of the emissivity of the original surface. Stefan-Boltzmann law describes heat exchange q_x in case of gray surface, where emissivity and absorptivity are equal:

$$q_x = \epsilon\sigma_{sb}A_1(T_1^4 - T_2^4). \quad (10)$$

In this equation, ϵ is emissivity, σ_{sb} is Stefan-Boltzmann's constant, A_1 is the area through which the heat exchange is calculated, T_1 and T_2 are absolute temperatures of radiative surface and surrounding surface. (Jiji, 2006, p. 8; Keinänen and Öberg, 1989, p. 12–13)

3.5 Material model

As told in chapter 2.5, most of the material properties have nonlinear behavior with alternative temperature. This nonlinearity has to be described in the material model used in analysis. In the material model definition, properties are given alternative values at corresponding temperatures from room temperature to melting temperature. The more values are given, the more accurate are the results. On the other hand, some properties vary less with temperature and can be expressed as constants in the material model. Usually density of the material, thermal conductivity, Poisson's ratio and specific heat are properties which can be considered as constants (Bhatti et al., 2015, p. 881–882). To keep computing times reasonable, one needs to consider which material properties are included into material model. Properties included to the material model of this work were density, elastic behavior (Young's modulus

and Poisson's ratio), thermal expansion, plastic behavior (yield stress with different plastic strain values), specific heat and heat conductivity.

In the material model of this work, nonlinear material properties were the same as in Bhatti et. al.'s (2015, p. 880-883) research. However, they didn't inform the relationship between stress and plastic strain at different temperatures. Stress - plastic strain -relationship used in this work was the same than in Helander's master's thesis (Helander, 2009, p. 41–42). In this material model, the stress was given values with zero plastic strain and with strain level of 0.06 at different temperatures. The stress was determined to grow linearly from the value corresponding to zero strain to 10 MPa greater value, where plastic strain value was 0.06. This means that the material model is almost ideal elastoplastic. The whole material model is presented in appendix 1 with physical constants and predefined fields used in analysis.

3.6 Coupled and uncoupled analysis

Thermal stress analysis is possible to execute as coupled or uncoupled analysis. In coupled analysis, only one analysis is executed, where both thermal and mechanical solution is solved simultaneously. In uncoupled analysis in turn, two separate analysis are executed. This means that thermal analysis is solved first and stress analysis based on the data from thermal analysis is executed after it. This method needs a few simplifications. At first, it's assumed that deformations and stress states do not affect to the thermal solution by relieving or consuming the heat energy. In reality, there is a slight coupling between them. Another simplification is that the deformations in the structure are so insignificant that they do not affect to heat conduction in the structure. (Brischetto and Carrera, 2010, p. 1793–1794; Eslampanah et al., 2015, p. 343; Kollár, Kövesdi and Nézo, 2017, p. 99) When AWI is used in Abaqus, the welding analysis is executed as uncoupled analysis.

3.7 Boundary conditions

Thermal boundary conditions are determined by equations 9 (convective heat transfer) and 10 (radiative heat transfer) which were introduced in chapter 3.4.2. When defining film properties i.e. convective heat transfer boundary conditions, AWI asks film coefficient and sink temperature, which is the temperature of the base material before welding. To define the boundary conditions of radiative heat transfer, AWI asks the emissivity of the material and

ambient temperature, which means the initial temperature of the model's environment. Used thermal boundary conditions are defined in table 2.

Table 2. Thermal boundary conditions

Convective heat transfer		Radiative heat transfer	
Film coefficient	Sink temperature	Emissivity	Ambient temperature
0.025	21.1	0.75	21.1

Due to advice of my supervisor, mechanical boundary conditions were fulfilled with adapted 3-2-1 rule of mechanical constrains. The idea of 3-2-1 –rule is to pick three points from the model. These points form a plane. Displacements of all three points are locked in one direction (for example x-direction). Then another direction (for example y-direction) of displacement is locked from two of these three points. The last point's displacement is then locked in the last direction (z-direction). With this method, rotation and displacement can be locked with minimum amount of restraints and deformation during welding is not excessively limited by constraints. The adaption of this rule means that the entire cutting plane of the model was locked in y-direction as it was represented in chapter 3.2. Otherwise, the rule was obtained. Locking the whole cutting plane in y-direction gives the model less capability to deform, but this was determined to be acceptable because the welds included to the analyses were far away from this plane. Used boundary constraints based on 3-2-1 –rule are shown in figure 11. (Cugnoni, 2009, p. 6–7)

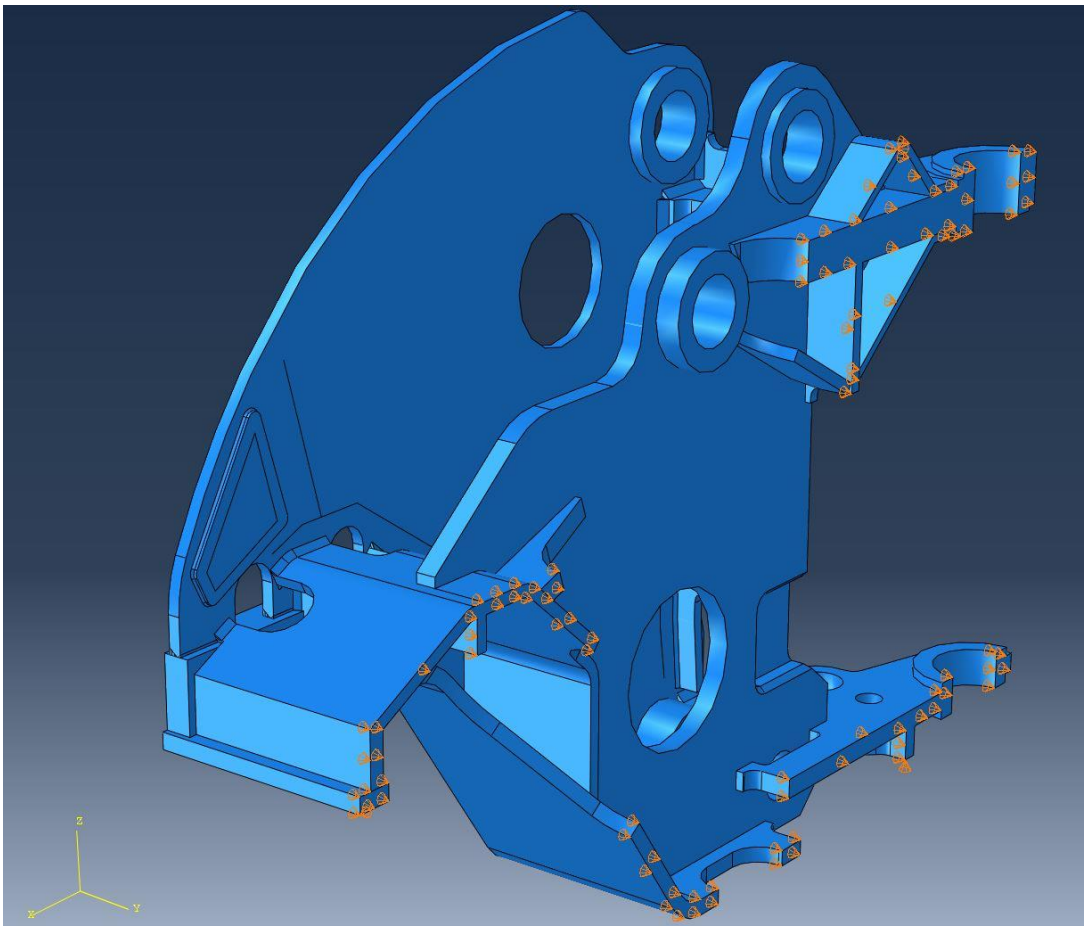

Figure 11. 3-2-1 rule -based mechanical constraints

3.8 Meshing of the part

Mesh density has a significant effect on accuracy of the analysis and computing times. If the mesh is too dense, computing times grow unnecessarily long, although the accuracy of the results are good. On the other hand, if the mesh is coarse, the computing time stay shorter but accuracy of the results may suffer. To keep balance between these two situations, the most reasonable way to produce a mesh in welding analysis is to create dense mesh to welds and their neighborhood, where strong stress states and plastic behavior of material are expected. Coarser mesh is acceptable further from the welds. (Manurung et al., 2013; Pu et al., 2017, p. 1217–1218)

This was the procedure used in creating mesh on the model. Ready mesh is presented in figure 12 where one can see the difference between fine mesh near the welds and coarse mesh further in the base material.

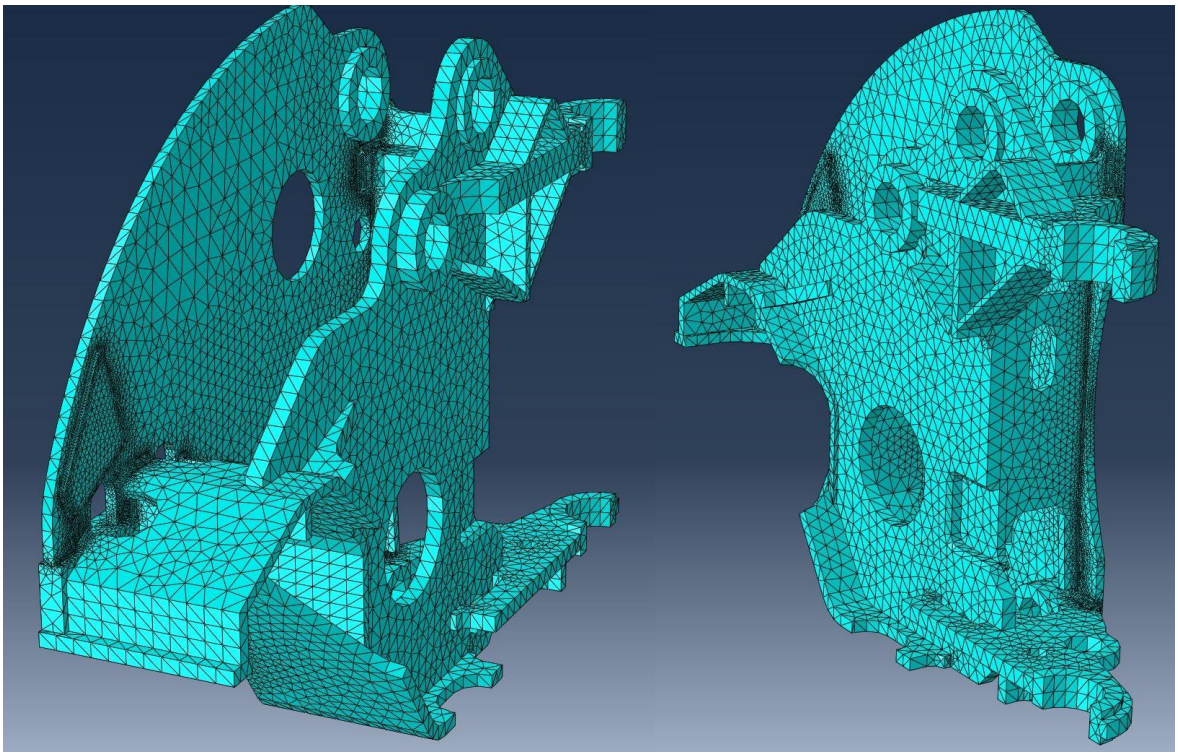

Figure 12. Finer and coarser mesh at different regions of the model

Different element shapes were tried during meshing of the model. At first the welds and few regions of the base material were meshed with hex elements and the rest of the model was meshed with tetra elements. In fine adjustment of the mesh it was noticed that mesh refinement was easier when all-tetra mesh was used. Hence, all the mesh was created with tetra elements. The total amount of elements was 166 805 in case of right half and 159 202 in case of left half so it was clear that analysis will be heavy and time-consuming. The element type in thermal analysis was DC3D4, which is a linear four-node heat transfer element. In stress analysis the element type was C3D4, which is also a four-node tetrahedron but a linear 3D stress element. The same mesh was used in both analyses.

3.9 Calibration of the parameters in finite element analysis

The parameters used in welding analysis were calibrated with welding tests. They were executed to three parts, which imitate a part of a real frame in a scale 1:1. They were welded with the same welding parameters as a real frame. Approximate welding parameters are shown in table 3.

Table 3. Approximate welding parameters

Bead	Filler wire thickness (mm)	Wire feed speed (m/min)	Welding current (A)	Arc voltage (V)	Welding speed (mm/s)	Heat input (kJ/mm)
Root pass	1.2	13	285	33.5	5	1.52
Fill up pass	1.2	15	300	34.5	4	2.07
Final pass	1.2	16.5	340	35.5	3	3.21

A welding analysis was done to a similar model with the same welding sequence. Parameters in AWI were adjusted so that the deformations were same in reality and in welding analysis. Specimen welded in the test and 3D-model of them are shown in figure 13. Welding sequence is also marked to the figure of the model. Drawing and the dimensions of the weld test specimen are presented in appendix 2.

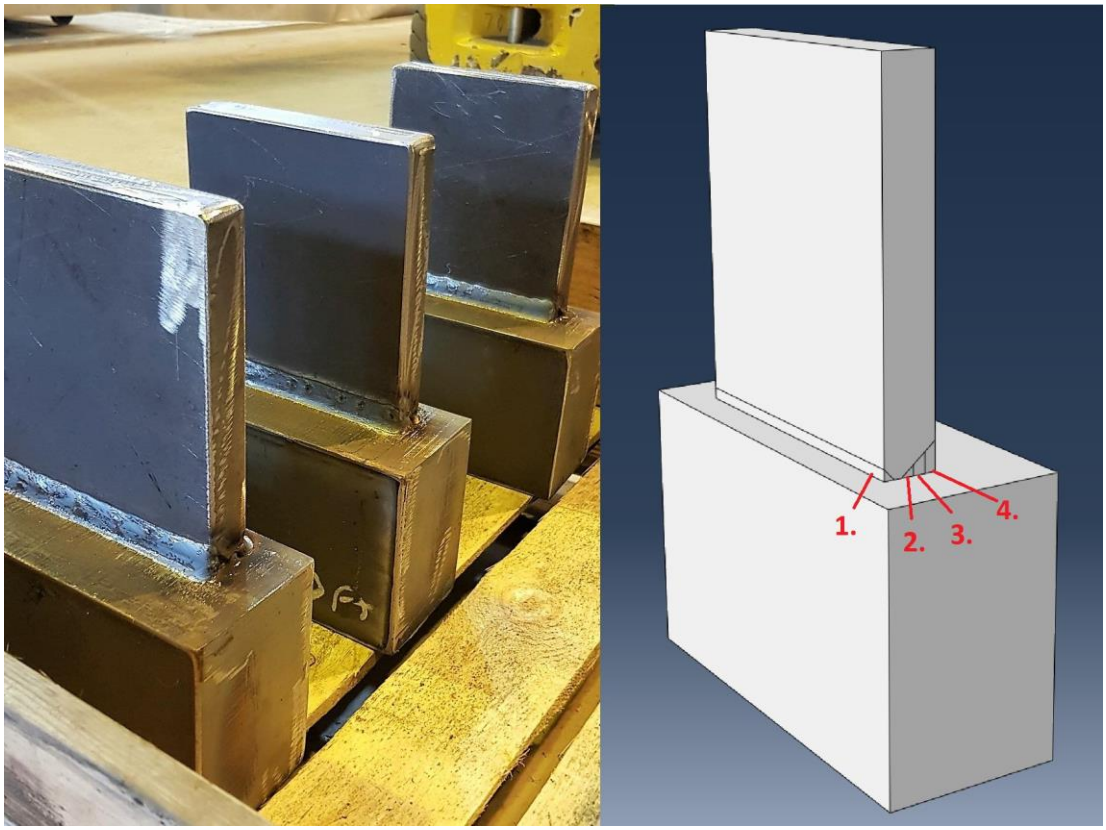

Figure 13. Test welded specimen for calibrating and the model of them

Welding distortions were measured from these specimen. Most important welding distortion type was angular distortion. It was measured simply by comparing the distances of thinner plate's upper and lower edges from the plane of the thicker plate's side. Measuring procedure is shown in figure 14. The direction of angular distortion was towards the side with bigger weld (illustrated in figure 14). It was ensured after tack welding that there was no angular distortion and the distance was 20 mm at both upper and lower edge. Table 4 presents the measured values of angular distortion *U*.

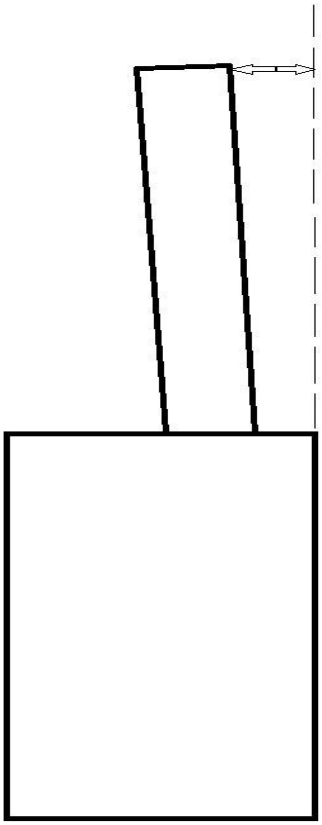

Figure 14. Measuring of angular distortion

Table 4. Values of angular distortion in test welded specimen.

Specimen (number)	Distortion value U (mm) at the ends and at the middle of the upper edge		
	Measuring point 1 (left end)	Measuring point 2 (center)	Measuring point 3 (right end)
1	3.4	3.9	3.7
2	3.9	3.8	3.8
3	0.4	0.8	0.7
Average	2.7		
Average of 1 and 2	3.8		

As one can see, the angular distortion was significantly smaller in the third specimen. The reason to this was that the first weld bead, which should be a flat faced weld, was more like fillet weld and had greater capability to prevent angular distortion formed by that bigger weld welded after it. Hence, parameters were calibrated to correspond the average distortion of specimen 1 and 2. In the analysis of the test welds, displacements were investigated at same areas as they were measured in the real specimen; at both ends and at the middle of the upper edge. In Abaqus, it is possible to plot the displacement of arbitrary nodes of elements. Figure 15 shows the nodal displacement in x –direction as a color coded map. The nodes, which were included in plotting of displacement, are highlighted with blue rings. Figure 16, in turn, shows their value of displacement in x-direction during welding analysis. The distortion rates of all the three nodes are plotted but their values are so similar that they look like one graph. Displacement in x-direction is corresponding to angular distortion in this case. Other distortion types were so insignificant that they were excluded. Table 5 contains the parameters determined by the calibration.

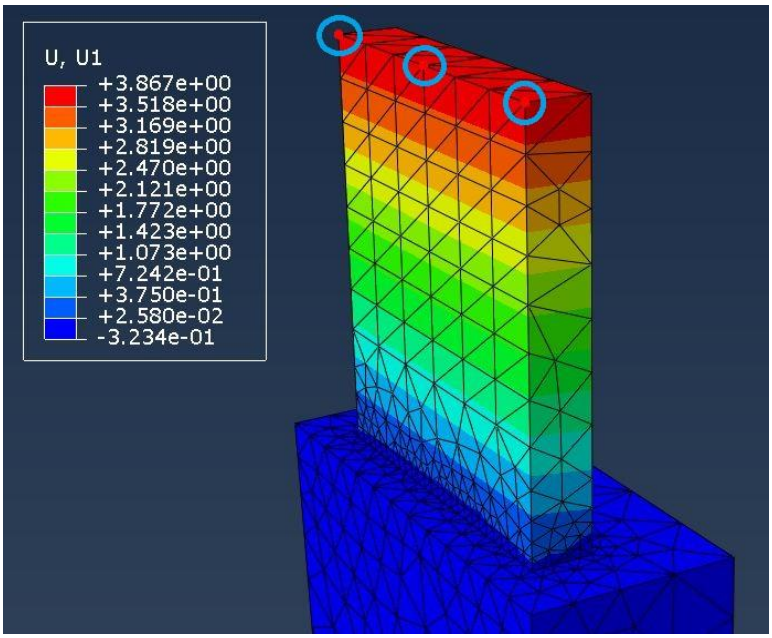

Figure 15. Nodal displacement in x-direction and the nodes which displacement was plotted.

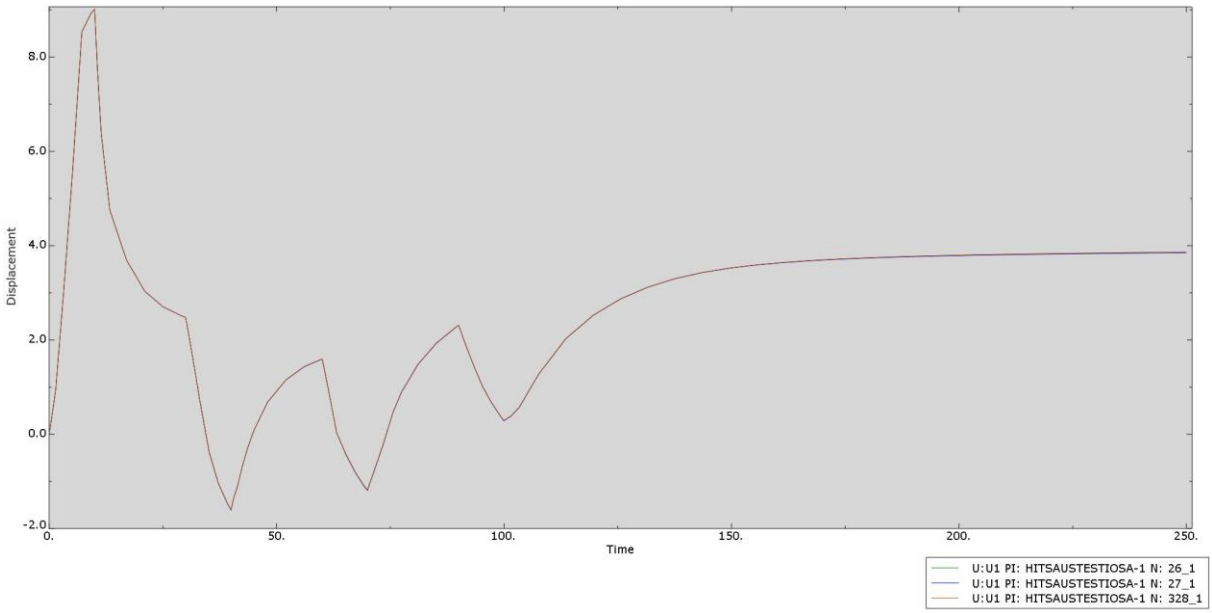

Figure 16. Displacement of the nodes during welding

Table 5. Parameters used in analysis.

Weld Attributes		
	Weld material initial melt temperature	1525 °C
	Target torch heat up temperature	1300 °C
Pass Step Controls		
Apply torch step	Time period of inserting a bead	10 s
	Initial, min. and max. time increments	0.1 s, 1 x 10^{-5} s, 1 s
	Max. number of increments	1000
	Max allow. temp. change	100 °C
	Heating ramp length	7 s
	Max temp holding time	3 s
Cool down step	Min. cooling time between passes	30 s
	Cooling time after last pass	150 s
	Initial, min. and max. time increment	0.1 s, 1 x 10^{-5} s, 1 s
	Max number of increments	1000
	Max. allow. temp. change	100 °C
Film properties	Film coefficient	0.025 mJ/s/mm^2/K
	Sink temperature	21.1 °C
Radiation properties	Emissivity	0.75
	Ambient temperature	21.1 °C

It was also investigated if computing time could be reduced by combining beads inside a weld if they are welded sequentially so that no other welds are welded between same weld's beads. The analysis of the calibration model was driven with the same parameters while two last beads were combined and they were laid down in the same step. There was only 2.3 % divergence between the results, so this simplification was used also in the analysis of the front frame's model. However, this simplification only applies to beads, which are welded sequentially, not all beads.

3.10 Analyzing cases with variable welding sequences

This chapter introduces the welding sequences, which were analyzed in Abaqus. Analyzed welding sequences are numbered from 1 to 9. Because the original welding sequence was not equal in side plates, it was analyzed in two phases (sequences 1 and 2). Sequence number one is the original welding sequence of the right side plate and number two is the original sequence of the left side plate. The rest of the numbers are alternative sequences, with which the welding distortions were aspired to reduce. These alternative sequences are determined to be identical in both side plates. Hence, only one analysis is needed per sequence and it's driven with the model of the right side plate. First welding sequence is presented in figure 17. It's the original sequence of the right side plate.

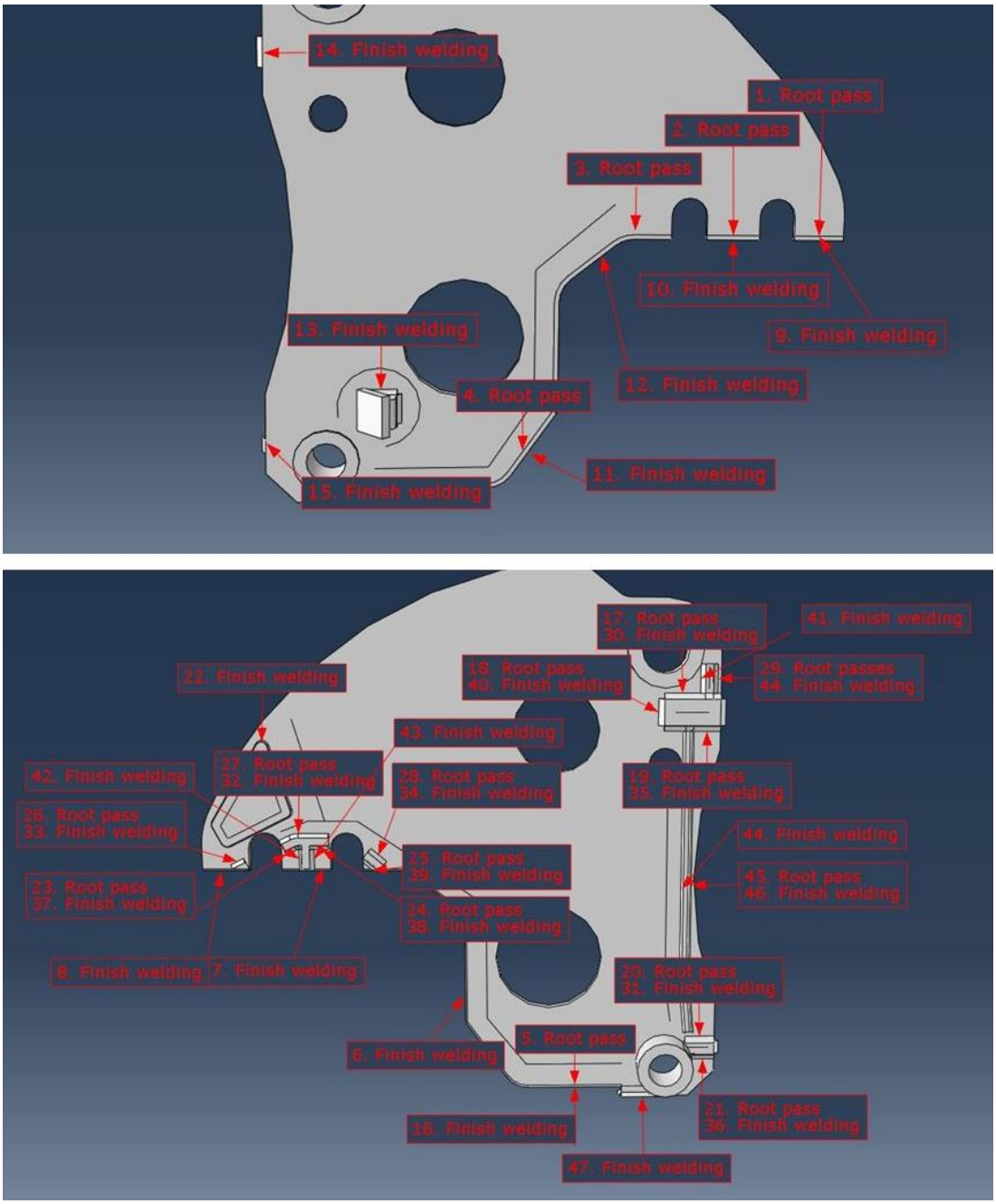

Figure 17. Original welding sequence of the right side plate (sequence 1).

The second analysis was driven for the left half of the model with original welding sequence (sequence 2). This sequence is shown in figure 18. The most important difference between these two sequences is that the abrasion resistant plate was welded earlier in the left side plate (in phase 17 instead of phase 22).

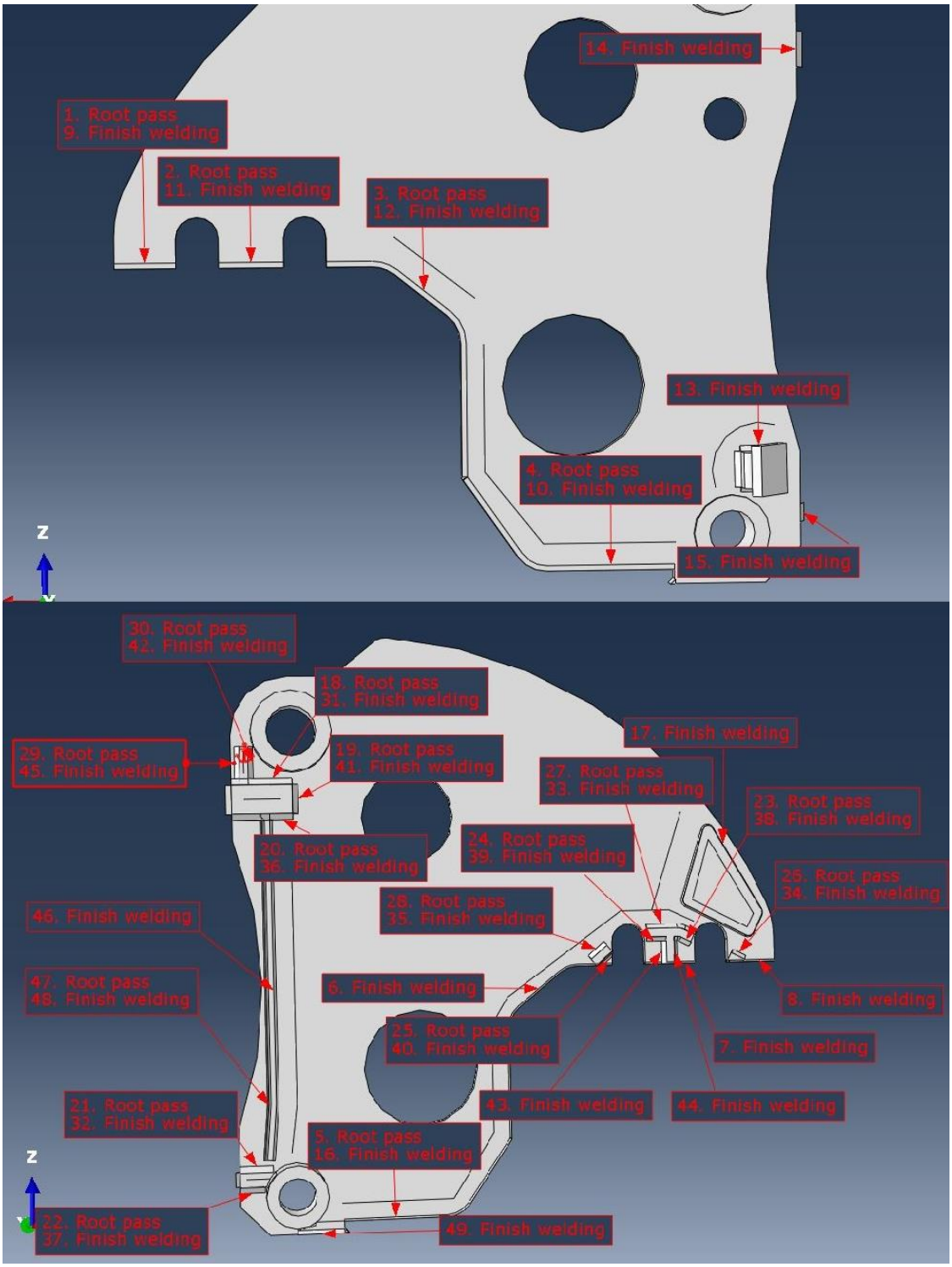

Figure 18. Original welding sequence of left side plate (sequence 2).

Figure 19 represents the welding sequence 3. In this sequence the welds inside the lower frame are welded before those welds which are inserted outside the lower frame. This can be seen if comparing the phases 22-42 of both sequences. The purpose of this sequence is

that the side plate could bloat outwards and gain more stiffness before welds 40-41 are welded. Welds 40-42 strongly pull the side plate inwards.

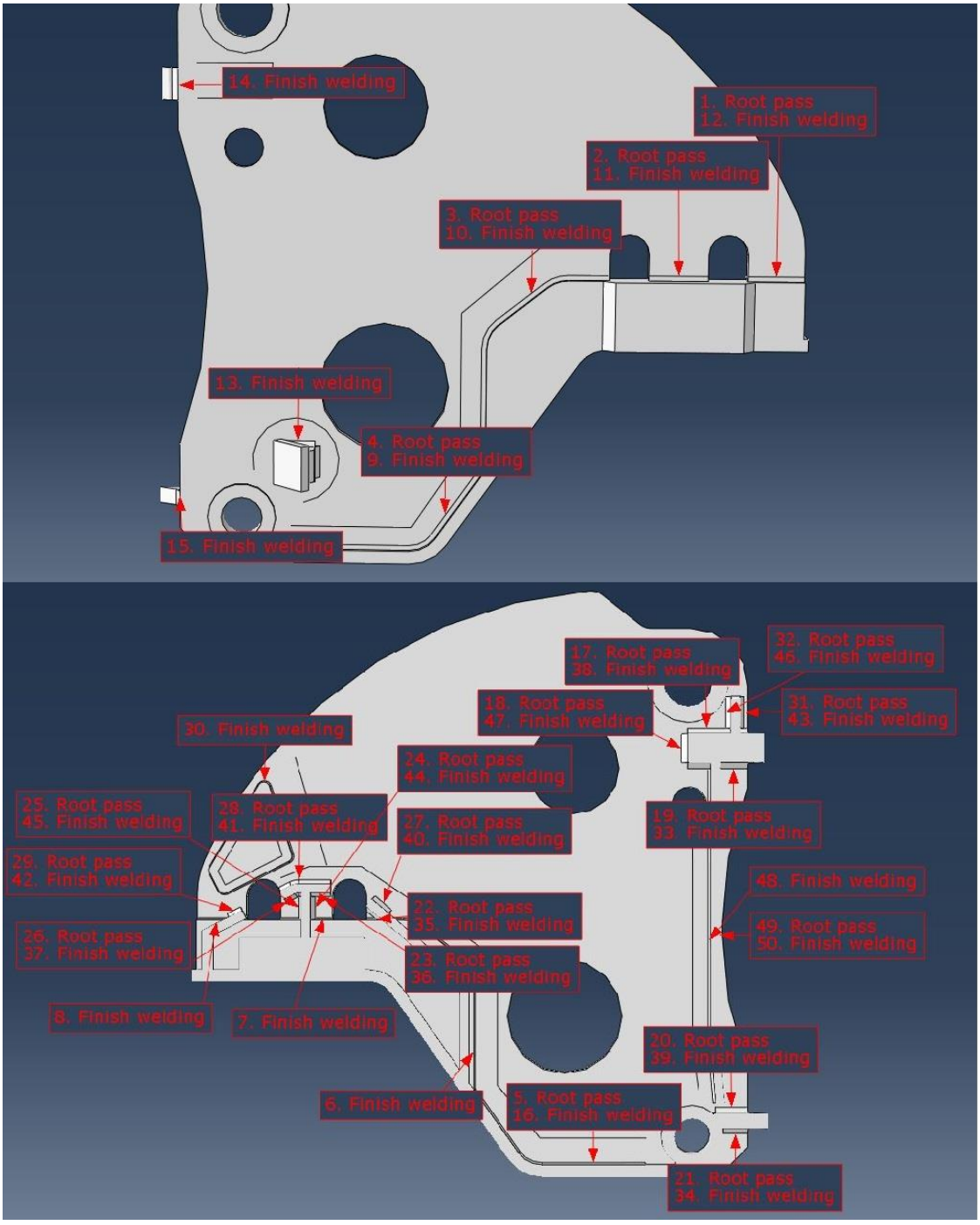

Figure 19. First alternative welding sequence, sequence 3.

Figure 20 introduces the welding sequence 4. In this sequence, phases 22-42 of sequence 3 were nearly turned upside down because the sequence 3 produced even greater distortions

than the two original welding sequences. In this sequence, welds outside the lower frame were welded before the inner ones. Again, this can be seen from the phases 22-40.

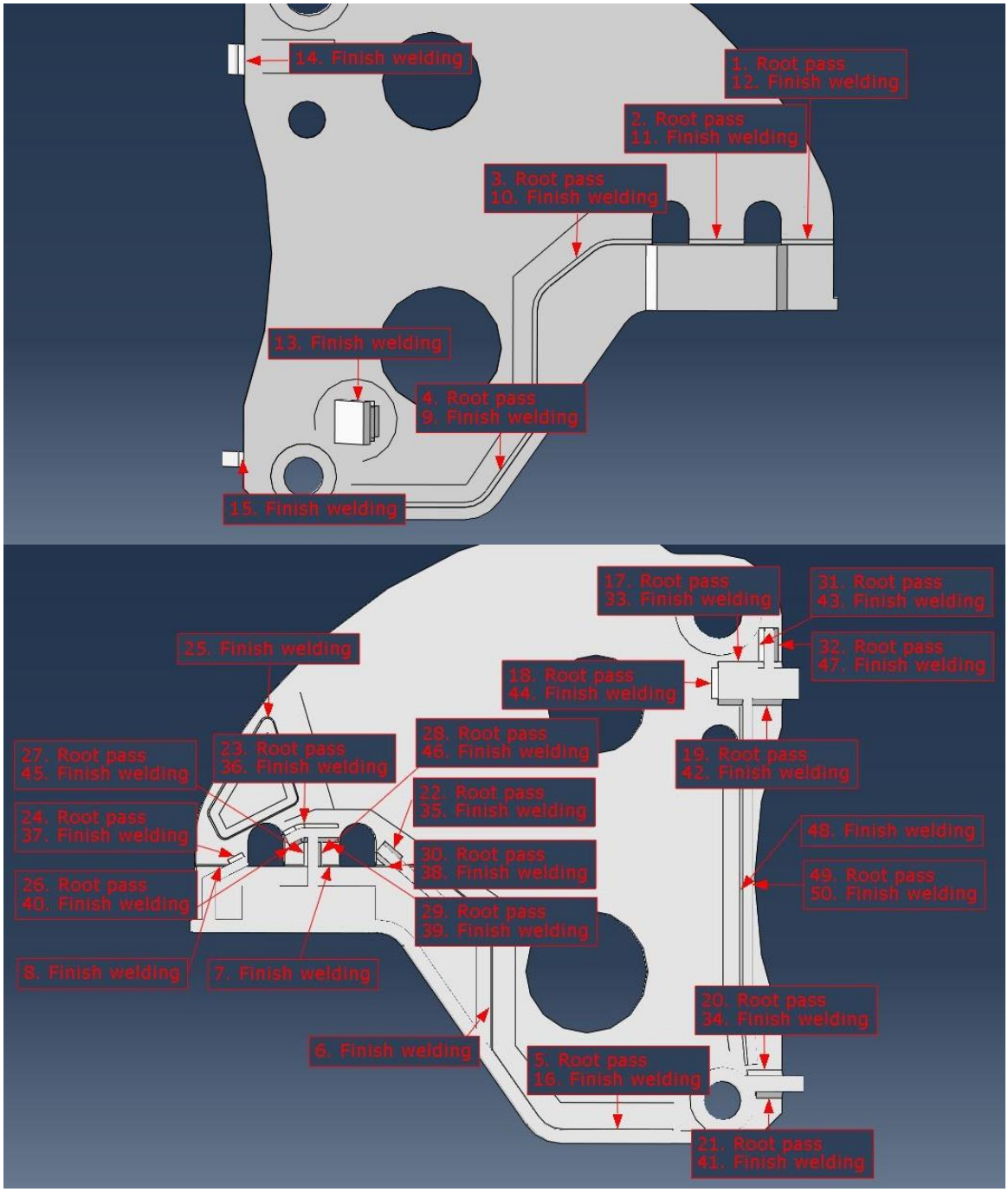

Figure 20. Welding sequence 4.

Welding sequence 5 is presented in figure 21. This sequence was intentionally planned as the worst sequence to investigate what is the greatest possible value of distortion when welded with the same welding parameters. In this sequence all the welds outside the side

plate, with the exception of the phases 1-4 (root passes), were inserted as late as possible. Those welds outside the side plate are important in reducing the distortions that are pulling the side plate inwards because they are the only welds which pull the plate outwards. In this sequence, the welds 25-30 were welded in turns so that every second weld was welded outside the lower frame and every second inside of it. As expected, this sequence produced the greatest welding distortions.

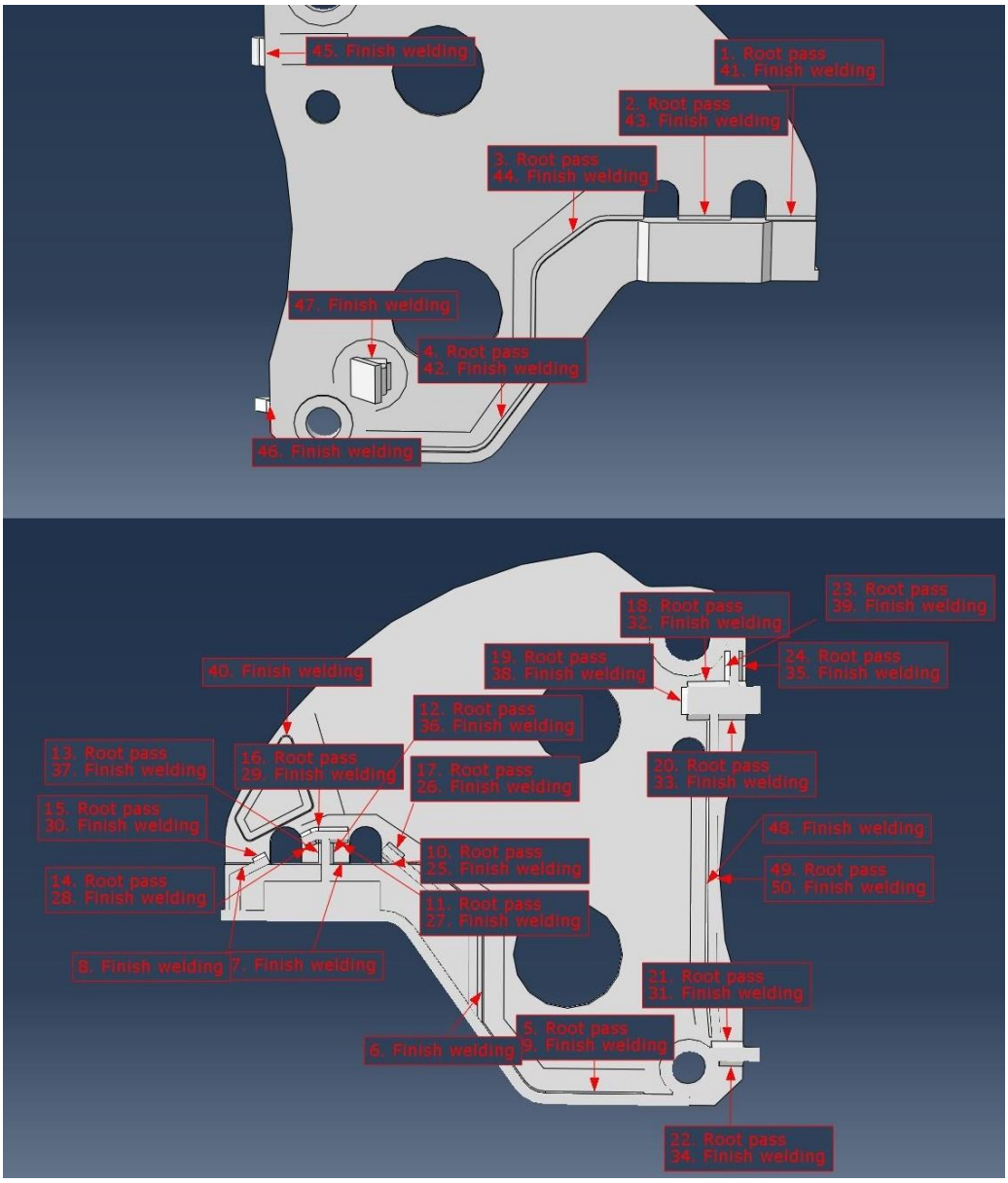

Figure 21. Welding sequence 5.

Welding sequence 6 (figure 22) was created as an opposite of welding sequence 5. All the welds of the side plate's outer surface were welded completely before any of the inner surface's welds. The purpose of this was to investigate if the side plate could bulge outwards in the beginning of the welding work when the stiffness of the structure is as it's lowest.

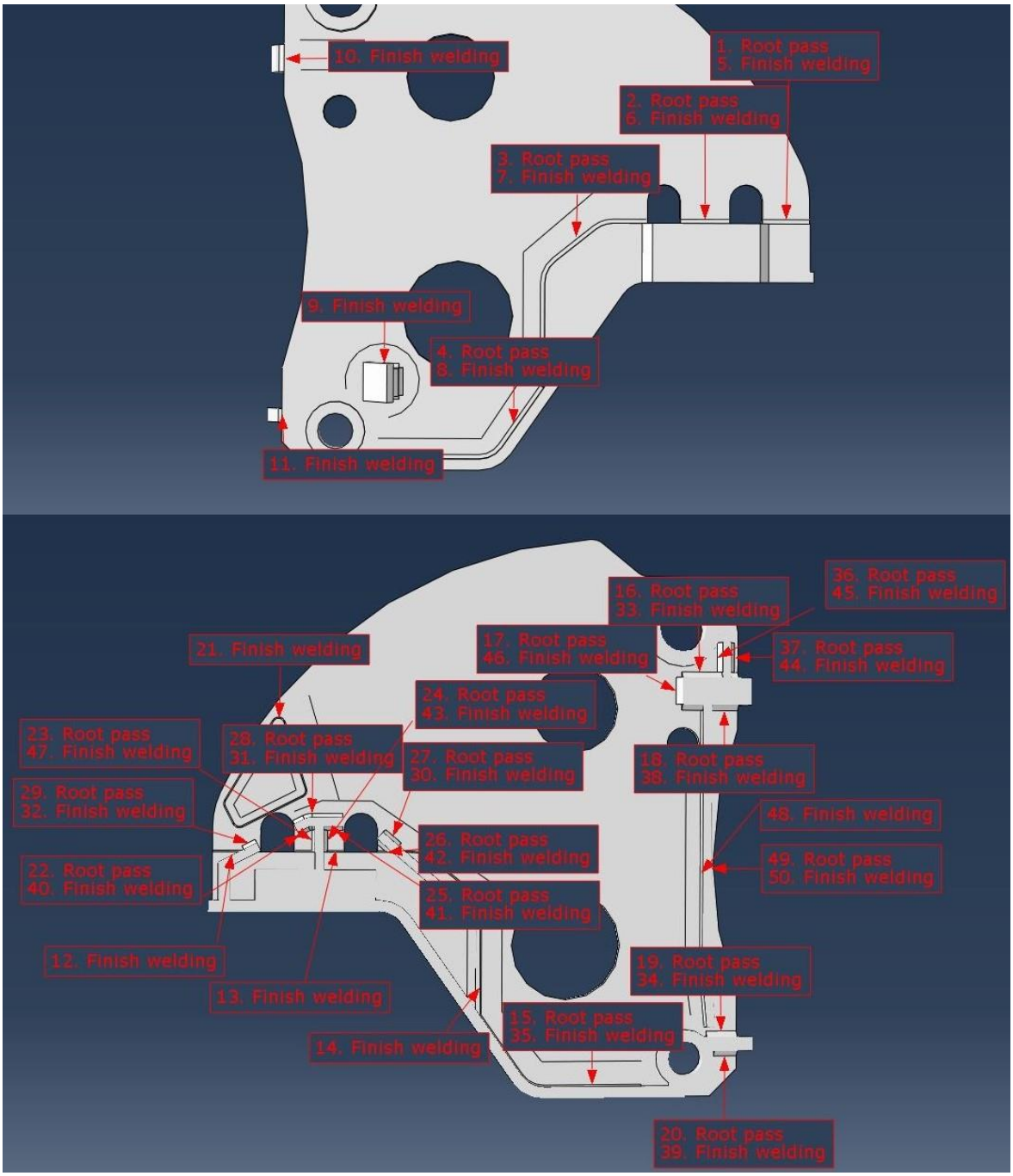

Figure 22. Welding sequence 6.

In sequence 7, it was investigated if the distortions are smaller when abrasion resistant plate is welded as early as possible and the joints inside the lower frame are welded before outer ones. Attention was also taken to the joints of upper hinge plate – weld under the plate was welded before upper one. The welding sequence 7 is presented in figure 23.

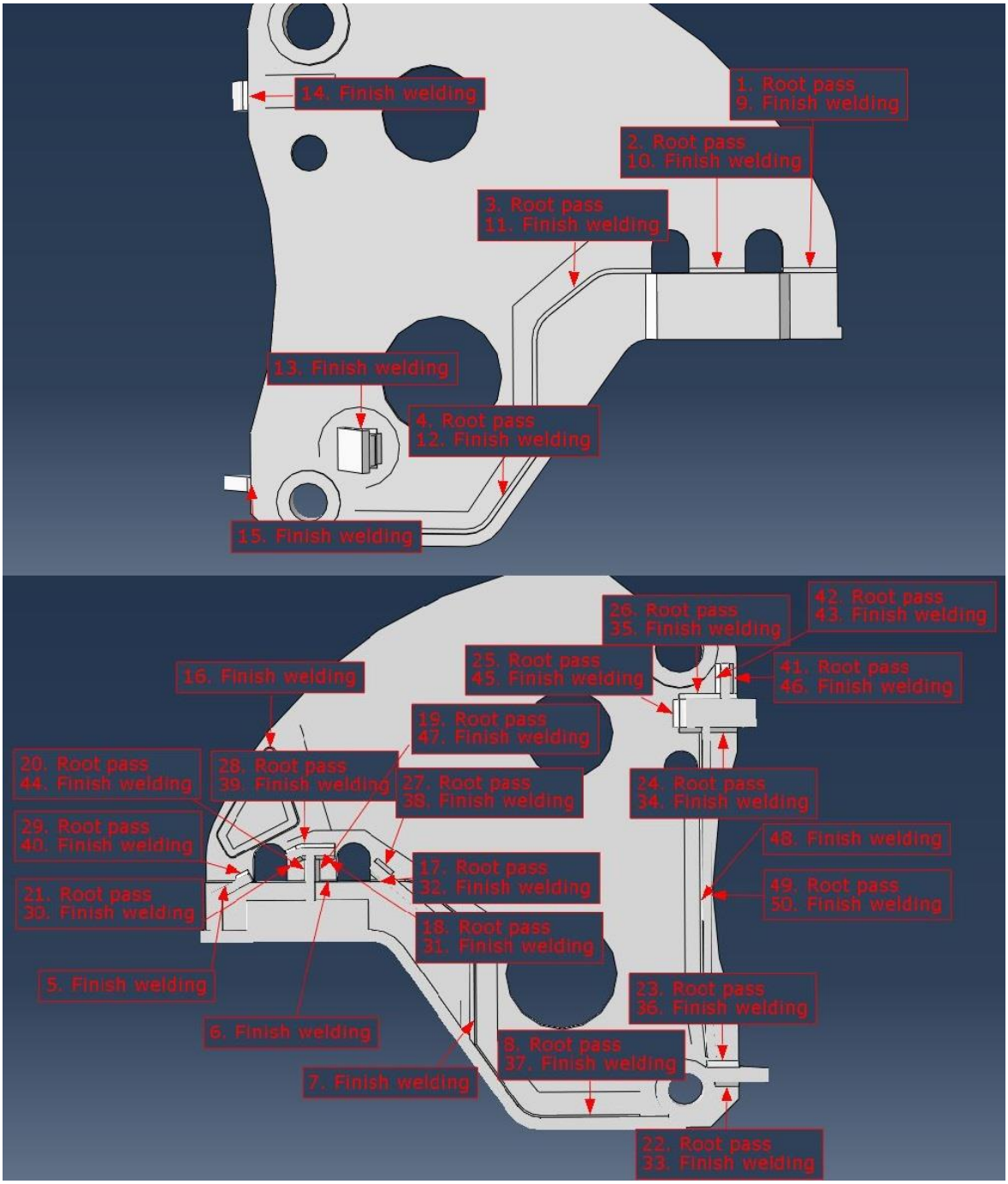

Figure 23. Welding sequence 7.

Welding sequence 8 (figure 24) was a combination of things that seemed to produce less distortions. These things seemed to be next ones:

1. Welds inside the lower frame were welded after outer ones
2. Abrasion resistant plate was welded as early as possible
3. Upper hinge plate's upper weld were welded before the lower one
4. Fillet weld between side plate and lower frame (phases 8 and 37 in sequence 7) was welded as early as possible

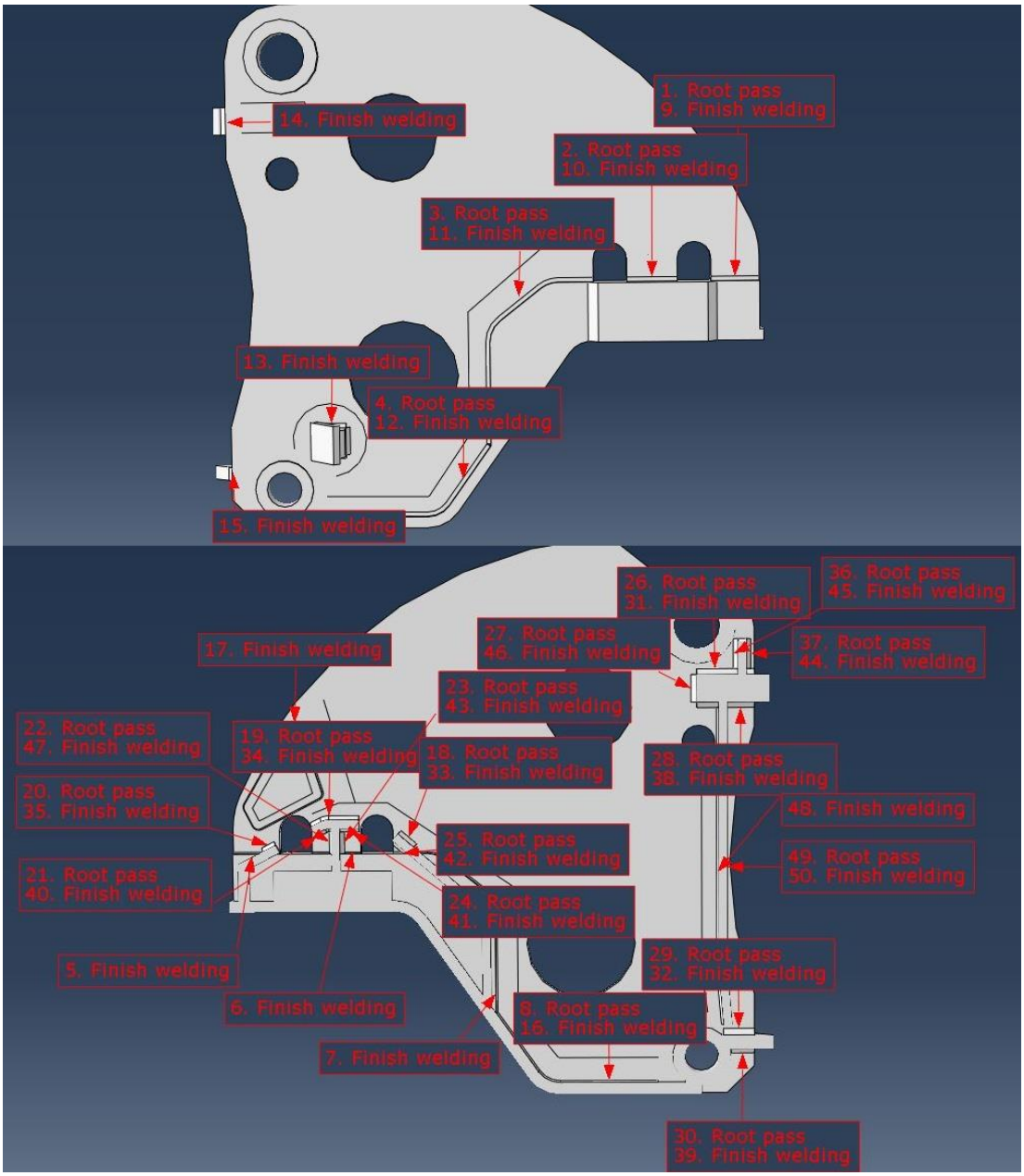

Figure 24. Welding sequence 8.

The result of sequence 8 was not what was expected. Distortions were still greater than with the two original sequences and sequence 4. Hence, one more welding sequence was created. In this sequence 9 (figure 25) the main differences to the sequence 8 lie around the hinge plate's and lower frame's joints to the side plate. In this case, those were welded so that their lower side's welds (roots and final passes) were welded before upper side.

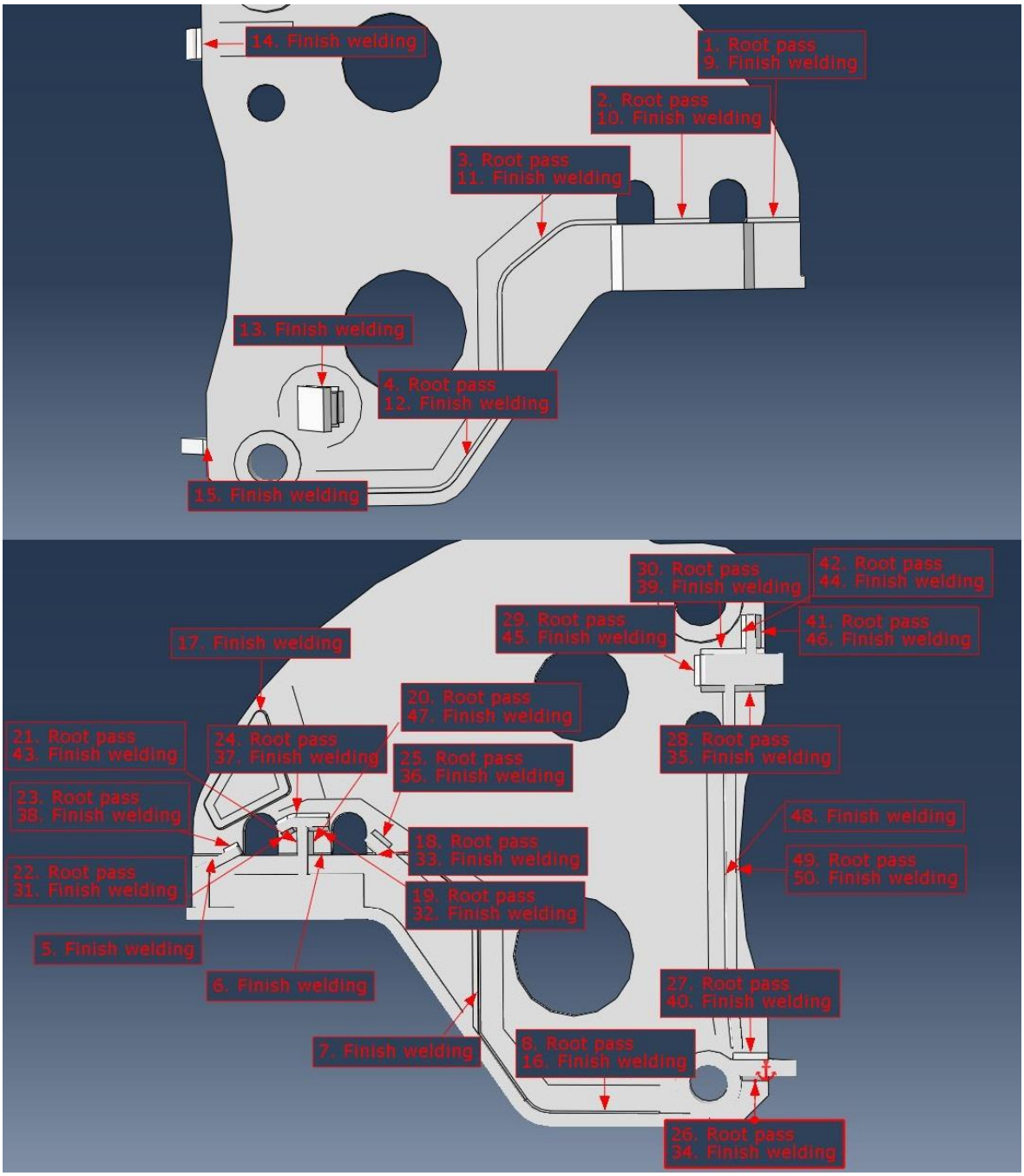

Figure 25. Welding sequence 9.

4 RESULTS

In this chapter the results of the analyses are introduced. The results are introduced in two ways. Firstly, as a figure of the model, where the final distortions after welding are presented as a color coded map with the scale of distortion value's and color's dependency. The figure represents the final distortion values after cooling time of 150 seconds. Because the distortions occur mostly in y-direction (normal to the side plate), the results are shown in that direction too. The second way of representing of distortions is plotting the displacement values of four nodes around the model as function of time. These four nodes are shown in figure 26 and are used in sequences 1 and 3-7. In sequence 2, which was the original welding sequence of the right side plate, the nodes are picked from corresponding locations of the model so that they are comparable. Figures of final welding distortions in the model and nodal displacement plots are presented in appendices 3-20.

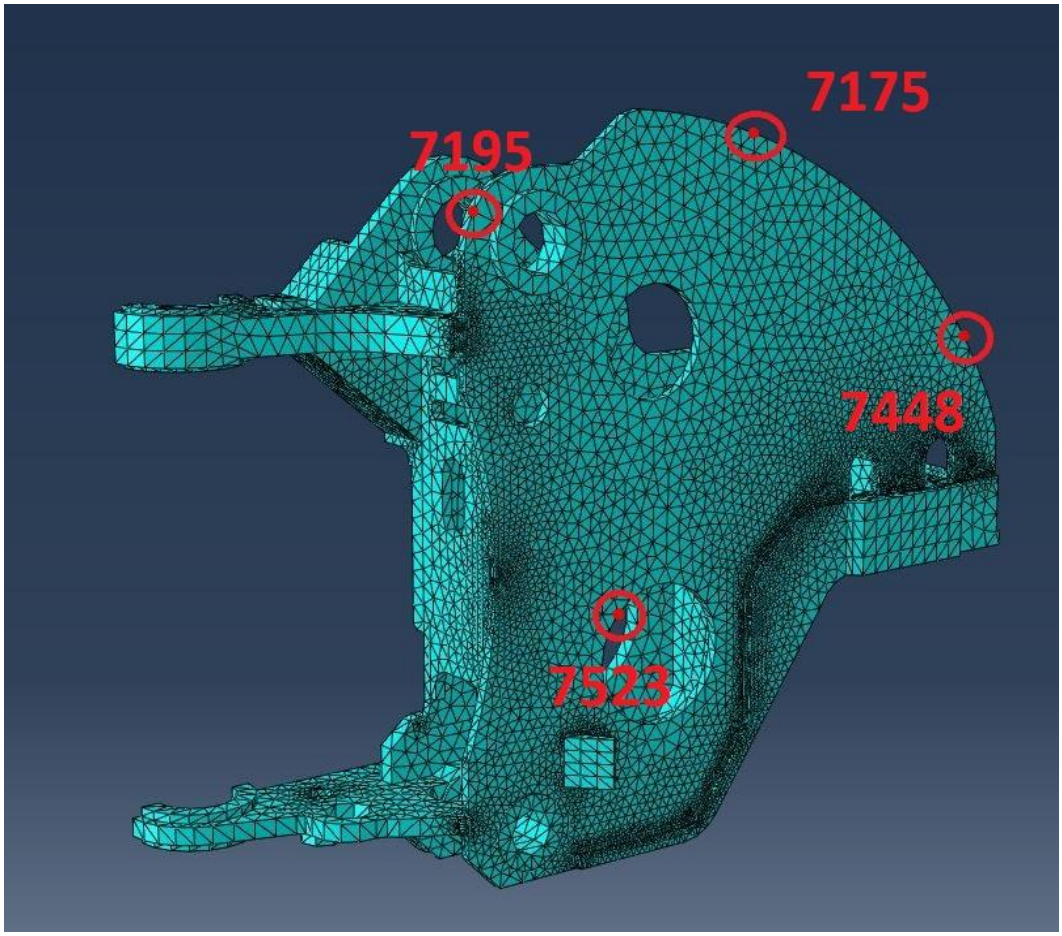

Figure 26. Nodes which displacement during welding are plotted.

Table 6 represents the final displacement value of the four nodes after cooling time. In case of sequence two, the node numbers are not correct but the values were taken from corresponding nodes of the other model.

Table 6. Final nodal displacements after cooling time in each welding sequence.

	Displacement after cooling (mm)			
	Node 7175	Node 7195	Node 7448	Node 7523
Sequence 1	2,5	0,5	0,8	-0,8
Sequence 2	2,3	0,6	0,8	-0,8
Sequence 3	2,8	0,75	0,9	-0,75
Sequence 4	2,5	0,6	0,85	-0,75
Sequence 5	3,5	1,2	1,0	-1,0
Sequence 6	3,25	1,0	0,9	-0,4
Sequence 7	2,75	0,75	0,85	-0,75
Sequence 8	2,75	0,6	0,95	-0,75
Sequence 9	2,75	0,7	0,85	-0,75

When comparing the results of the analyses with the measured deformations of the real welded frame (figure 7), it is noticeable that the volume of the distortions is higher in measured frame, especially in the left side plate. There is at least two reasons for this difference. Firstly, the frame was fastened to a welding positioner from it's right side plate. This may have caused different forces to the structure during welding work, when the frame was turned several times into different positions. The other remarkable reason to greater distortions is that many supporting bars were mounted between the frame plates during welding process. Those bars were inserted with help of hydraulic press, which may have caused more deformations. Neither of these were not taken into account in the analyses. However, the shape and the direction of the welding distortions are quite similar in both measured frame and the results of the analyses. Due to this, the results can be considered reliable.

4.1 Comparison of welding distortions in case of each welding sequence

As one can see from the table 6, node 7175 has greatest distortion value in each welding sequence. This is because it has the greatest capability to move along the welding distortions

- even a small angular distortion at the side plate's and lower frame's joint displaces the upper edge significantly. It can be noticed commonly with every welding sequence that the value of the distortion is smaller at lower regions of the side plate than higher.

Sequences 1, 2 and 4 produced the smallest distortions at nodes 7175, 7195 and 7448. The difference is clearest at nodes 7175 and 7195. Sequence 6 produced the smallest distortion at node 7523 but the divergence between sequences at that node is insignificant. Because of this the sequences were compared mostly by inspecting the distortion values of nodes 7175 and 7195 which lie on the top of the side plate and have the greatest distortion values hence.

The area around node 7448 is one of the most important to avoid excessive welding distortions because the lifting arm, which is mounted later, can easily hit the abrasion resistant plate too heavily. Of course, the side plates should not be excessively pulled inwards anywhere else neither so the lifting arm fits between the side plates.

4.2 Consideration of the results

After investigating the distortion values of each welding sequences, it seems that the three most convenient sequences were sequences 1, 2 and 4. Sequence 2 produced smallest distortions at node 7175 but the difference compared to sequences 1 and 4 is not very large.

The original welding sequences have also an advantage that they are the fastest ones to weld the front frame. This is because in those sequences every possible welding pass is welded when the frame is turned to each position. This leads to a minor amount of turning phases and improves the lead time for its part. More turning phases are required in every alternative welding sequences so they are not appropriate at that point of view neither.

The most important thing in comparing the sequences was the values of the distortions. An observation was also given to the shape of the welding distortion but it was quite similar with every tested welding sequence. This can be seen in appendices 3 – 20. Every second of those appendices represent the evolving process of the welding distortion values at nodes presented in figure 26. As one can see, the welding distortions reach almost the same value irrespective for the welding sequence.

5 CONCLUSIONS

Due to the results of the analyses, the two original welding sequences are the most appropriate ones from the list of the alternative welding sequences. Their privileges are not only the smallest welding distortions but also the lead time because the number of turning phases is at its minimum. It seems that in this structure is no possibility to get any smaller distortions by modifying the welding sequence only.

The most unfavorable thing to do when welding the structure is to weld every single weld from the other side of the side plate before the other. This was implemented in sequences 5 and 6 and those were the ones with greatest value of welding distortions. The problem is that the angular distortion grows and grows when all the beads are welded on the same side of the plate one after another. At the same time, the stiffness of the joint and structure increases and it's difficult to compensate the distortion by welds on the other side later.

When welding the lower frame to the side plate it seemed to not have any privileges if passes were welded in turns so that every other pass was welded outside of the lower frame and every other inside of it. This would have been very laborious operation in practice, too.

Based on this research it's obvious that finite element method is a convenient tool for reducing welding distortions even if it was not possible in this case. There would be considerably more ways to reduce distortions by editing the welding sequence if the structure has welds more symmetrically along it. In this case, the main problem is that there is many times more welds on the inner surface of the side plate than on the outer surface. The joint of lower frame's top and the side plate's inner surface is also higher than the outer surface's and lower frame's joint. This means that welds on the outer surface have not capability enough to pull the side plate completely back outwards.

The two inner frame plates are so thick and stiff in LH621's front frame that they didn't form welding distortions worth mentioning. Anyway, the interior of the frame would have been an excellent object to this research, if it had greater deformations but it didn't. The interior

of the frame has its welds more symmetrically than the side plates, which makes it more convenient for controlling welding distortions by welding sequence.

Abaqus 2017 were used in this study with Abaqus Welding Interface –plug-in. The plug-in is logical and fast to use after getting friends with it. However, the pre-work with the model is very time-consuming, especially if the geometry is complicated. The most arduous phase of the pre-work is meshing of the model. Controlling the density of the mesh could be easier in Abaqus. User can give element size for volumes, for example for welds and base material. Element growth from the welds towards the base material is very arduous to control because user has to create huge amount of partitions to create a reasonable mesh on this kind of model.

5.1 Further research

In this case, it was not possible significantly reduce welding distortions with alternative welding sequence, but finite element method could be a powerful tool for investigating the effect of heat input on welding deformations. It would be easier and more accurate with new AWI Pro to model welding process. The possibility for adjusting the heat source with voltage, welding current and welding should make it an efficient and accurate way to investigate the effect of heat input. Of course, the software could be any other too if it has features versatile enough to adjust the heat source.

Also, number of weld passes comes to the question with adjusting the heat input, because addition of the filler material varies when welding parameters are edited. As it was told in table 1, limiting the number of weld beads is one way to reduce angular distortion. However, it may be difficult to reduce the number of the beads from current number, because welds should be welded with higher heat input. It seems that with current welding parameters the heat input is close to the upper limit of S355 steel. Moreover, raising heat input raises angular distortion, which is at variance with limiting the number of weld beads.

REFERENCES

Bhatti, A. A., Barsoum, Z., Murakawa, H. and Barsoum, I. (2015) Influence of thermo-mechanical material properties of different steel grades on welding residual stresses and angular distortion, *Materials & Design (1980-2015)*, 65(Supplement C), pp. 878–889.

Brischetto, S. and Carrera, E. (2010) Coupled thermo-mechanical analysis of one-layered and multilayered plates, *Composite Structures*, 92(8), pp. 1793–1812.

Creaform (2018) Discover the best measuring arm. Yours., [online] Available at: https://www.creaform3d.com/en/metrology-solutions/optical-3d-scanner-metrascan (Accessed 23 April 2018).

Cugnoni, J. (2009) [PDF] Symmetry & boundary conditions - Free Download PDF, *Nanopdf.com*, [online] Available at: https://nanopdf.com/download/symmetry-amp-boundary-conditions_pdf (Accessed 13 April 2018).

Dassault Systèmes SIMULIA Corporation Inc. (2014) Abaqus Welding Interface (AWI) User's Manual, Dassault Systèmes SIMULIA Corporation Inc.

Deng, D., Murakawa, H. and Ma, N. (2012) Predicting welding deformation in thin plate panel structure by means of inherent strain and interface element, *Science and Technology of Welding and Joining*, 17(1), pp. 13–21.

Eslampanah, A. H., Aalami-aleagha, M. E., Feli, S. and Ghaderi, M. R. (2015) 3-D numerical evaluation of residual stress and deformation due welding process using simplified heat source models, *Journal of Mechanical Science and Technology*, 29(1), pp. 341–348.

Feng, Z. (2005) *Processes and mechanisms of welding residual stress and distortion*, CRC Press.

Goldak, J. A. and Akhlangi, M. (2005) *COMPUTATIONAL WELDING MECHANICS*, 233 Spring Street, New York, NY 10013, USA, Springer Science + Business Media, Inc, [online] Available at: https://link.springer.com/content/pdf/10.1007%2Fb101137.pdf (Accessed 27 March 2018).

Goldak, J., Chakravarti, A. and Bibby, M. (1984) A new finite element model for welding heat sources, *Metallurgical Transactions B*, 15(2), pp. 299–305.

Helander, J. (2009) Asennushitsauksen aiheuttamien muodonmuutosten arviominen propulsioyksikössä elementtimenetelmällä, Lappeenranta, Lappeenranta University of Technology.

Jia, X., Xu, J., Liu, Z., Huang, S., Fan, Y. and Sun, Z. (2014) A new method to estimate heat source parameters in gas metal arc welding simulation process, *Fusion Engineering and Design*, 89(1), pp. 40–48.

Jiji, L. M. (2006) *Heat convection*, Berlin ; New York, Springer.

Jun-mei, C., Hao, L., Jian-hua, W., Wei-xin, C. and Da-jun, H. (2005) Prediction of Welding Deformation With Inherent Strain Method Based On FEM, *Welding in the World*, (49), p. 7.

Keinänen, H. and Öberg, T. (1989) *Hitsausjännitysten ja -muodonmuutosten laskenta elementtimenetelmällä*, Espoo, Valtion teknillinen tutkimuskeskus (VTT).

Keivani, R., Jahazi, M., Pham, T., Khodabandeh, A. R. and Afshar, M. R. (2014) Predicting residual stresses and distortion during multisequence welding of large size structures using FEM, *The International Journal of Advanced Manufacturing Technology*, 73(1–4), pp. 409–419.

Kim, M., Kang, M. and Chung, H. (2015) Simplified welding distortion analysis for fillet welding using composite shell elements, *International Journal of Naval Architecture and Ocean Engineering*, 7(3), pp. 452–465.

Kollár, D., Kövesdi, B. and Nézo, J. (2017) Numerical Simulation of Welding Process - Application in Buckling Analysis, *Periodica Polytechnica. Civil Engineering; Budapest*, 61(1), pp. 98–109.

Lawson, R. M. and Newman, G. M. (1990) Fire resistant Design of Steel Structures - A Handbook to BS 5950: Part 8, The Steel Construction Institute.

Lee, J. M., Seo, H. D. and Chung, H. (2018) Efficient welding distortion analysis method for large welded structures, *Journal of Materials Processing Technology*, 256, pp. 36–50.

Lepola, P. and Ylikangas, R. (2016) *Hitsaustekniikka ja teräsrakenteet*, 1. Painos, Helsinki, Sanoma Pro Oy.

Lindgren, L.-E. and Hedblom, E. (2001) Modelling of addition of filler material in large deformation analysis of multipass welding, *Communications in Numerical Methods in Engineering*, 17(9), pp. 647–657.

Lindgren, L.-E., Runnemalm, H. and Näsström, M. O. (1999) Simulation of multipass welding of a thick plate, *International Journal for Numerical Methods in Engineering*, 44(9), pp. 1301–1316.

Lukkari, J. (2007) Työkaluja hitsauskoordinoijalle hitsauksen suunnittelua varten, *Hitsaustekniikka*, 57(2), p. 56.

Manurung, Y. H. P., Lidam, R. N., Rahim, M. R., Zakaria, M. Y., Redza, M. R., Sulaiman, M. S., Tham, G. and Abas, S. K. (2013) Welding distortion analysis of multipass joint combination with different sequences using 3D FEM and experiment, *International Journal of Pressure Vessels and Piping*, 111–112, pp. 89–98.

Murakawa, H., Luo, Y. and Koide, T. (1998) Inherent Strain and Its Application for Prediction of welding Deformation at Groove in Narrow Gap Welding, *Transactions of the JWRI (Japan Welding Research Institute)*, 21, pp. 61–67.

Park, J.-U., An, G., Woo, W. C., Choi, J. and Ma, N. (2014) Residual stress measurement in an extra thick multi-pass weld using initial stress integrated inherent strain method, *Marine Structures*, 39, pp. 424–437.

Pennala, E. (2000) *Lujuusopin perusteet*, 11th ed, Helsinki, Otatieto. Oy Yliopistokustannus University Press Finland.

Pillinger, I. (1992) The Elastic-Plastic Finite-Element Method, In *Numerical Modelling of Material Deformation Processes*, Springer, London, pp. 225–250, [online] Available at: https://link.springer.com/chapter/10.1007/978-1-4471-1745-2_9 (Accessed 29 March 2018).

Pu, X., Zhang, C., Li, S. and Deng, D. (2017) Simulating welding residual stress and deformation in a multi-pass butt-welded joint considering balance between computing time and prediction accuracy, *The International Journal of Advanced Manufacturing Technology*, 93(5–8), pp. 2215–2226.

Sandvik Mining & Rock Technology (2018) Sandvik Mining & Rock Technology — Sandvik LH621 High-Capacity, 21-Ton Loader For Maximum Productivity, [online] Available at: https://www.rocktechnology.sandvik/en/products/underground-loaders-and-trucks/advanced-underground-lhds/lh621-underground-lhd/ (Accessed 9 January 2018).

The Welding Institute (2011) Distortion - types and causes - Job Knowledge 33, [online] Available at: https://www.twi-global.com/technical-knowledge/job-knowledge/distortion-types-and-causes-033/ (Accessed 27 March 2018).

APPENDICES

Appendix I

Material model, physical constants and predefined fields in the Abaqus input file.

```
** MATERIALS
**
*Material, name=S355
*Conductivity
45.,  20.
35., 600.
28., 700.
34.,1400.
*Density
 7.85e-09,
*Elastic
210000.,  0.3,  20.
180000.,  0.3, 400.
100000.,  0.3, 700.
 60000.,  0.3, 790.
 30000.,  0.3, 900.
 10000.,  0.3,1000.
*Expansion
 1.2e-05,  20.
 1.6e-05,1400.
*Plastic
380.,   0.,  20.
390., 0.06,  20.
300.,   0., 500.
310., 0.06, 500.
 15.,   0., 800.
 25., 0.06, 800.
  5.,   0.,1400.
 15., 0.06,1400.
*Specific Heat
 5e+08,  20.
 9e+08, 700.
 6e+08, 900.
 7e+08,1400.
**
** PHYSICAL CONSTANTS
**
*Physical Constants, absolute zero=-273.15, stefan boltz-
mann=5.669e-11
**
** PREDEFINED FIELDS
**
** Name: WM_InitialBaseTemperature   Type: Temperature
*Initial Conditions, type=TEMPERATURE
LH261eturunko-1.Perusmateriaali, 21.1
** Name: WM_Weld-1_InitialTemperature   Type: Temperature
*Initial Conditions, type=TEMPERATURE
LH261eturunko-1.WM_Weld-1_InitialTemperature, 1525.
```

Appendix II

Drawing of the weld test part used in calibration.

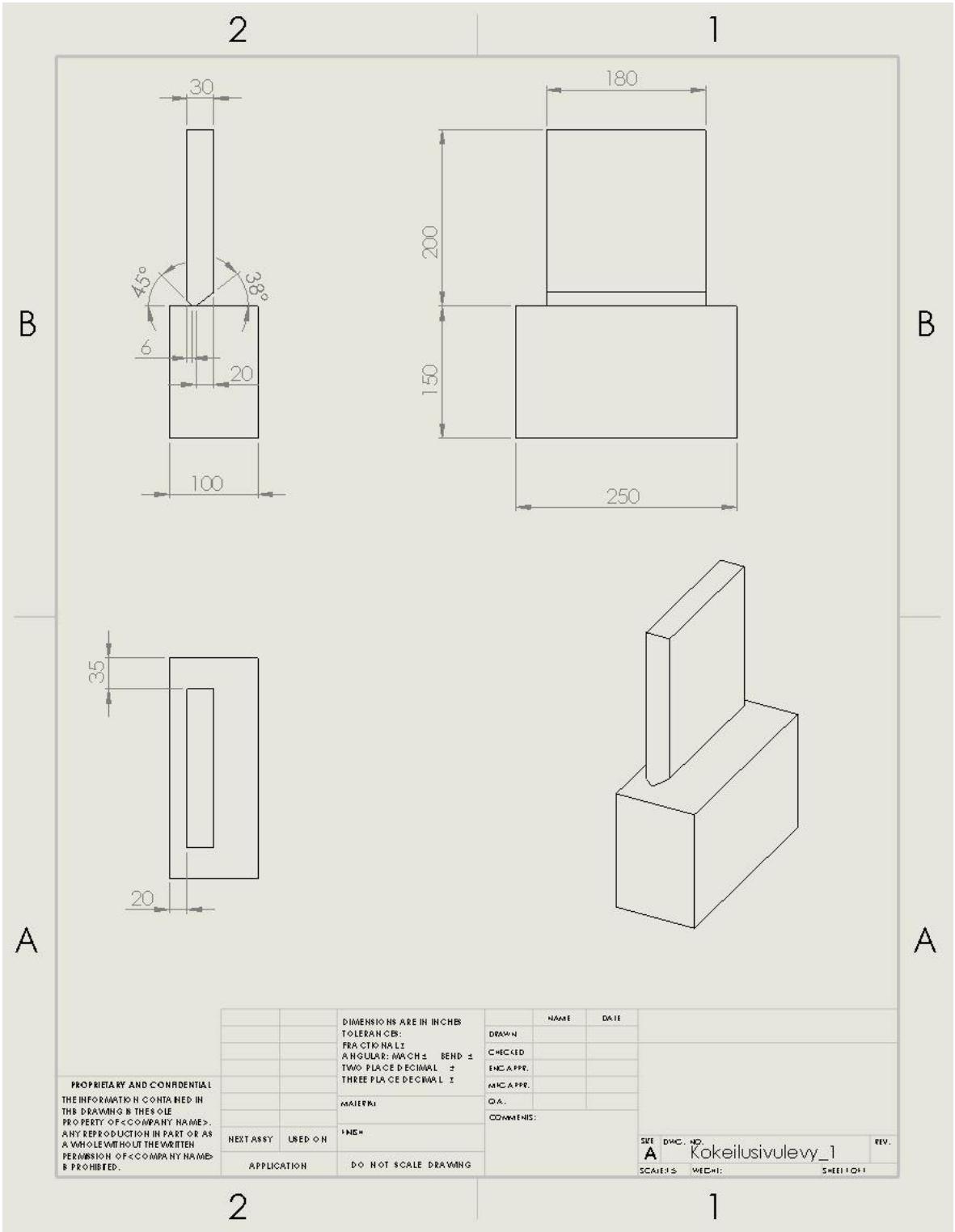

Appendix III

Nodal displacement of selected nodes during welding with welding sequence 1

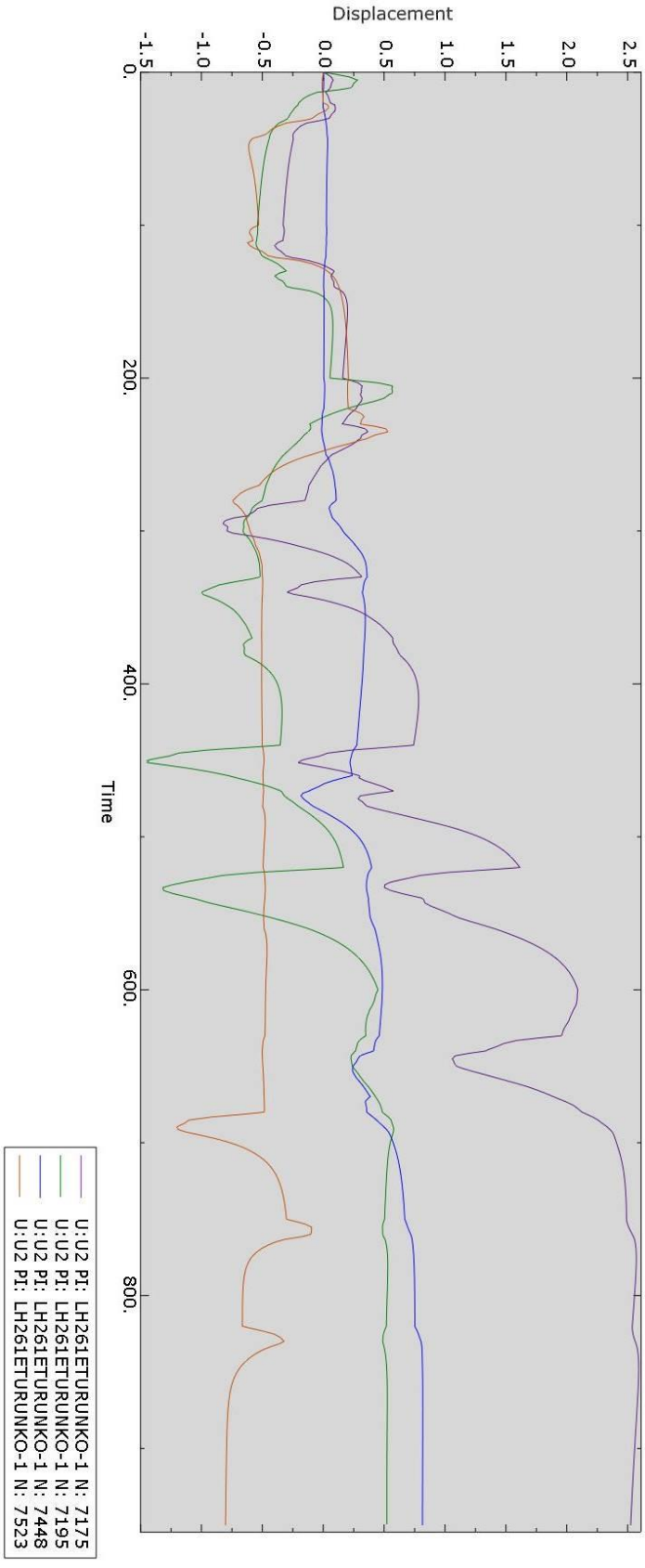

Appendix IV

Final welding deformations of welding sequence 1

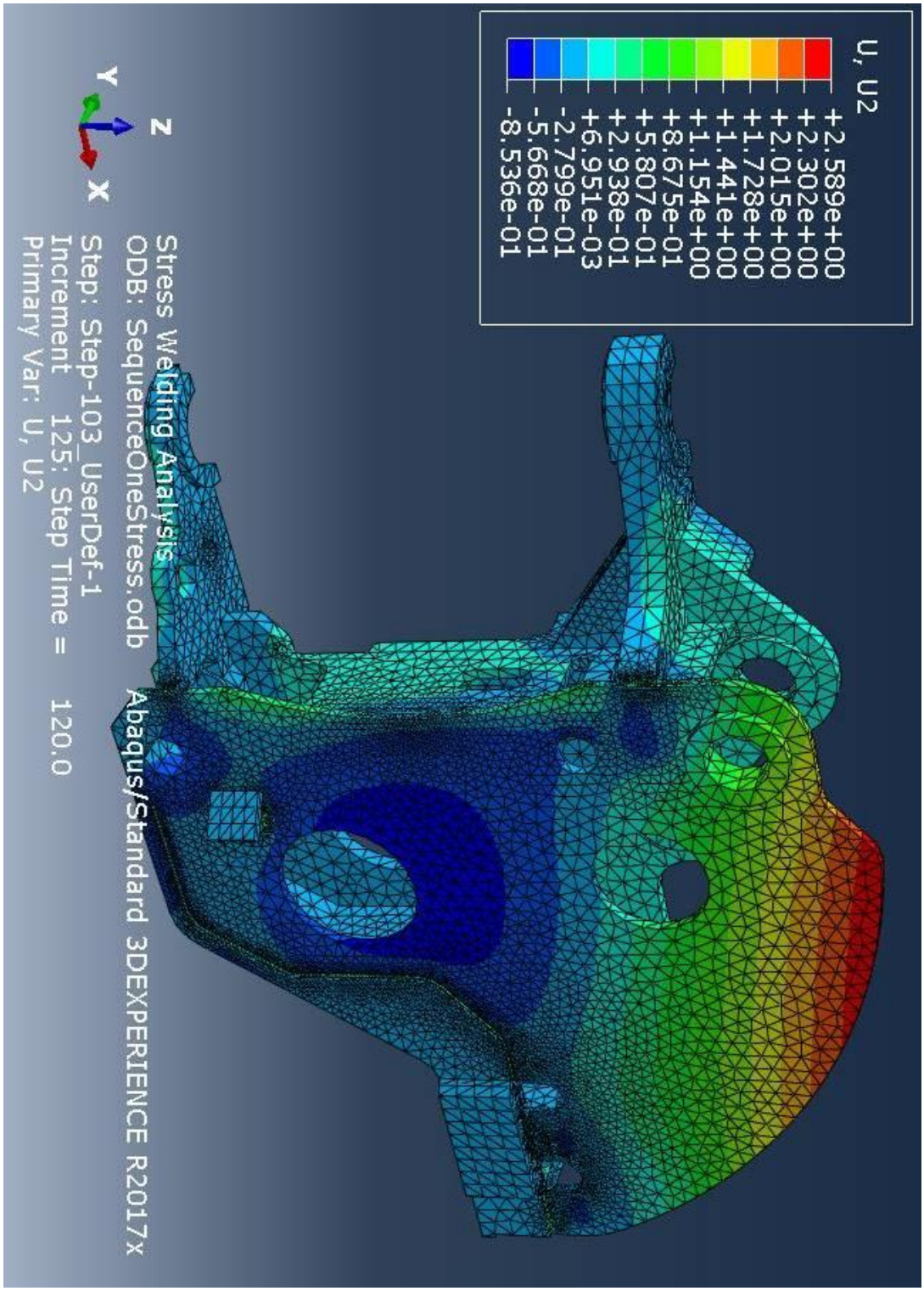

Appendix V

Nodal displacement of selected nodes during welding with welding sequence 2

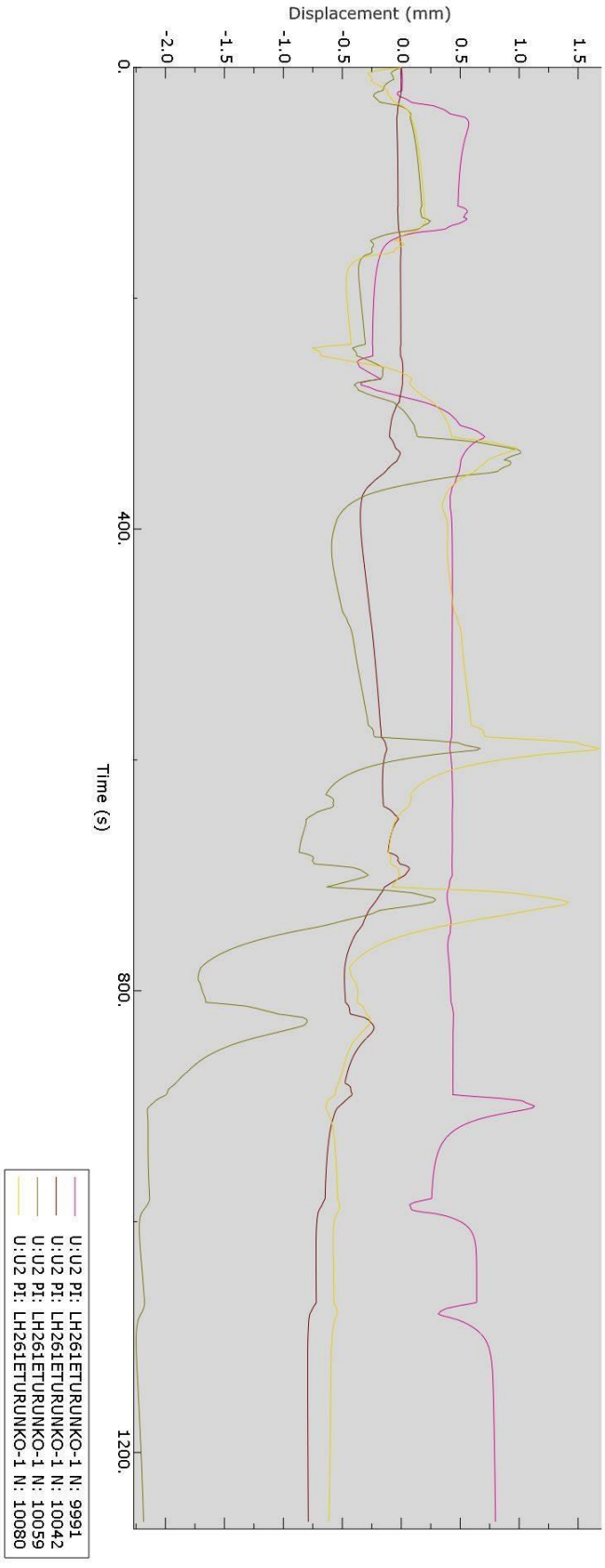

Appendix VI

Final welding deformations of welding sequence 2

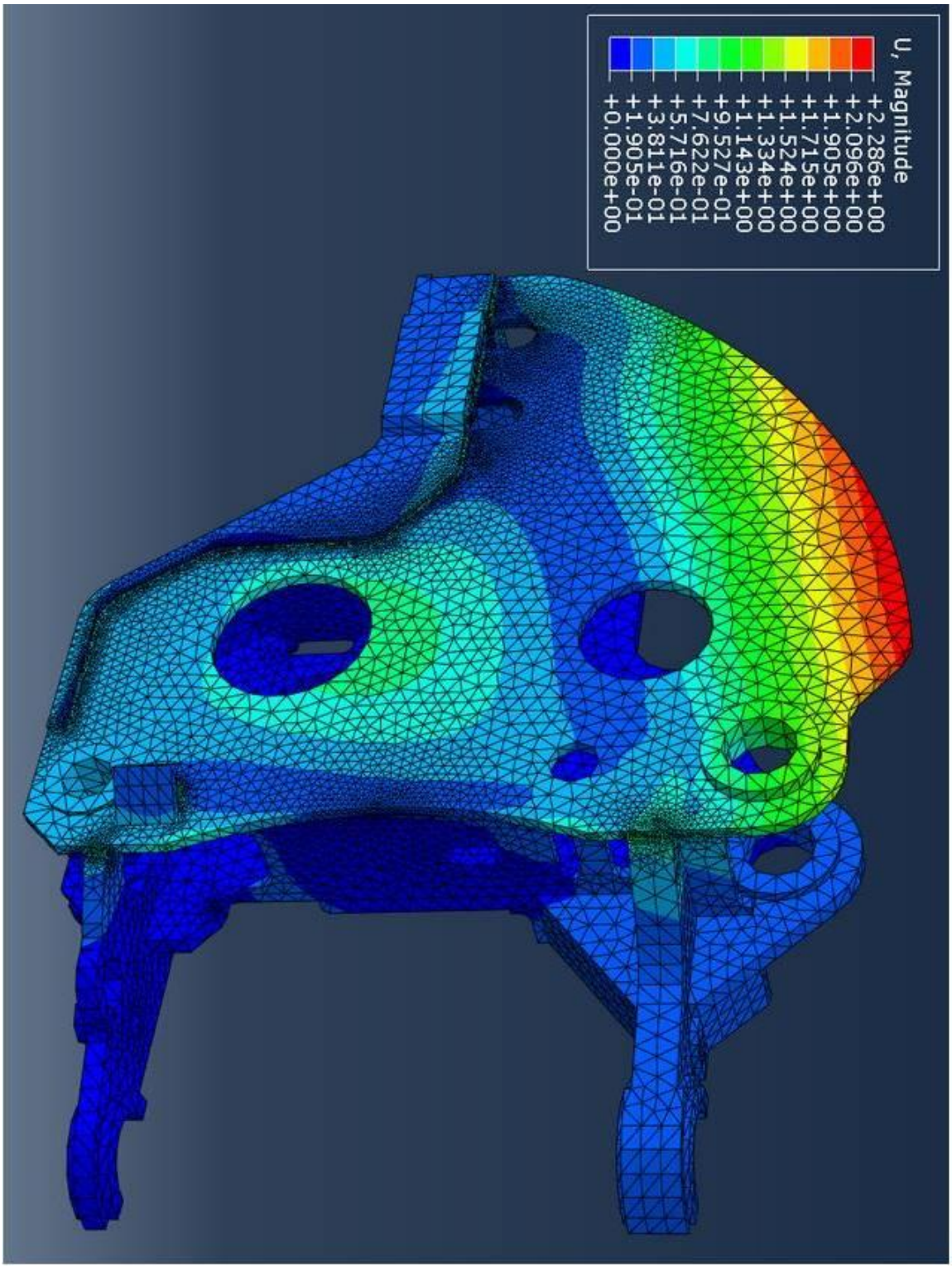

Appendix VII

Nodal displacement of selected nodes during welding with welding sequence 3

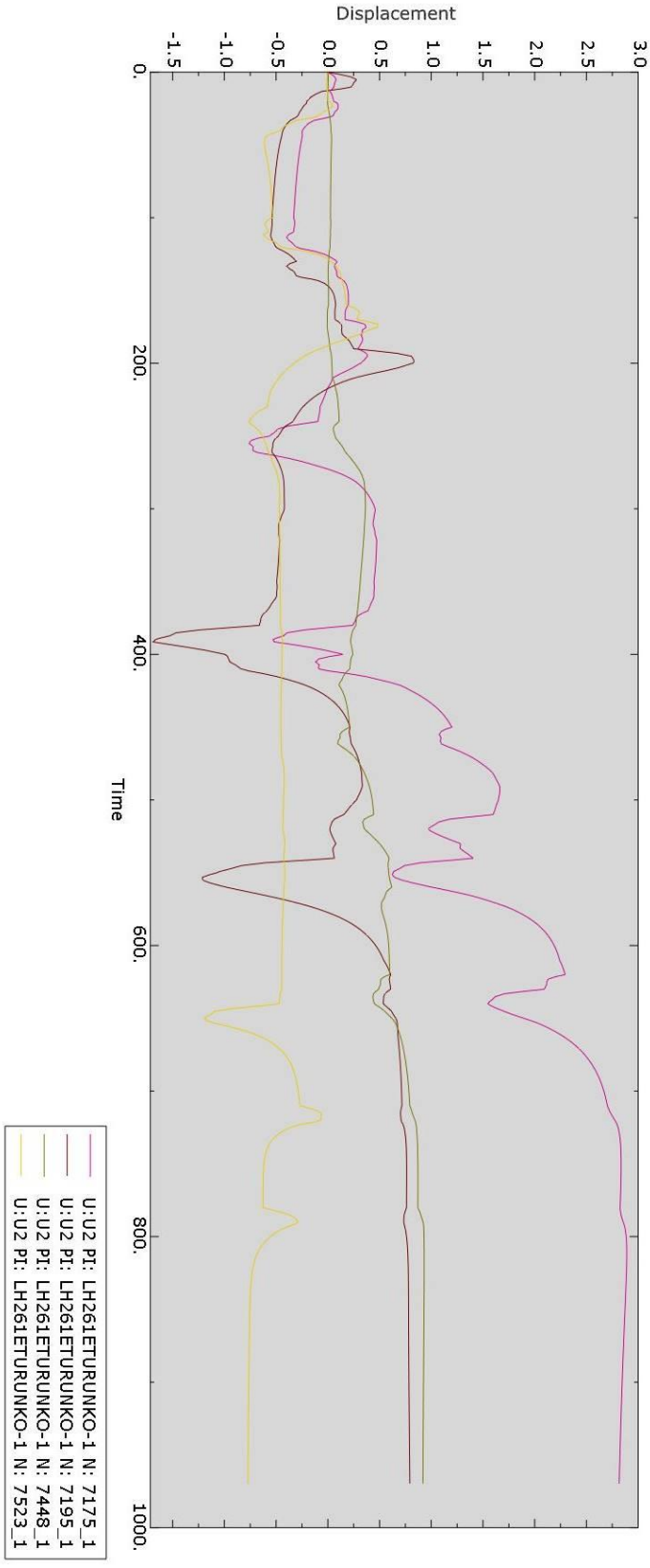

Final welding deformations of welding sequence 3

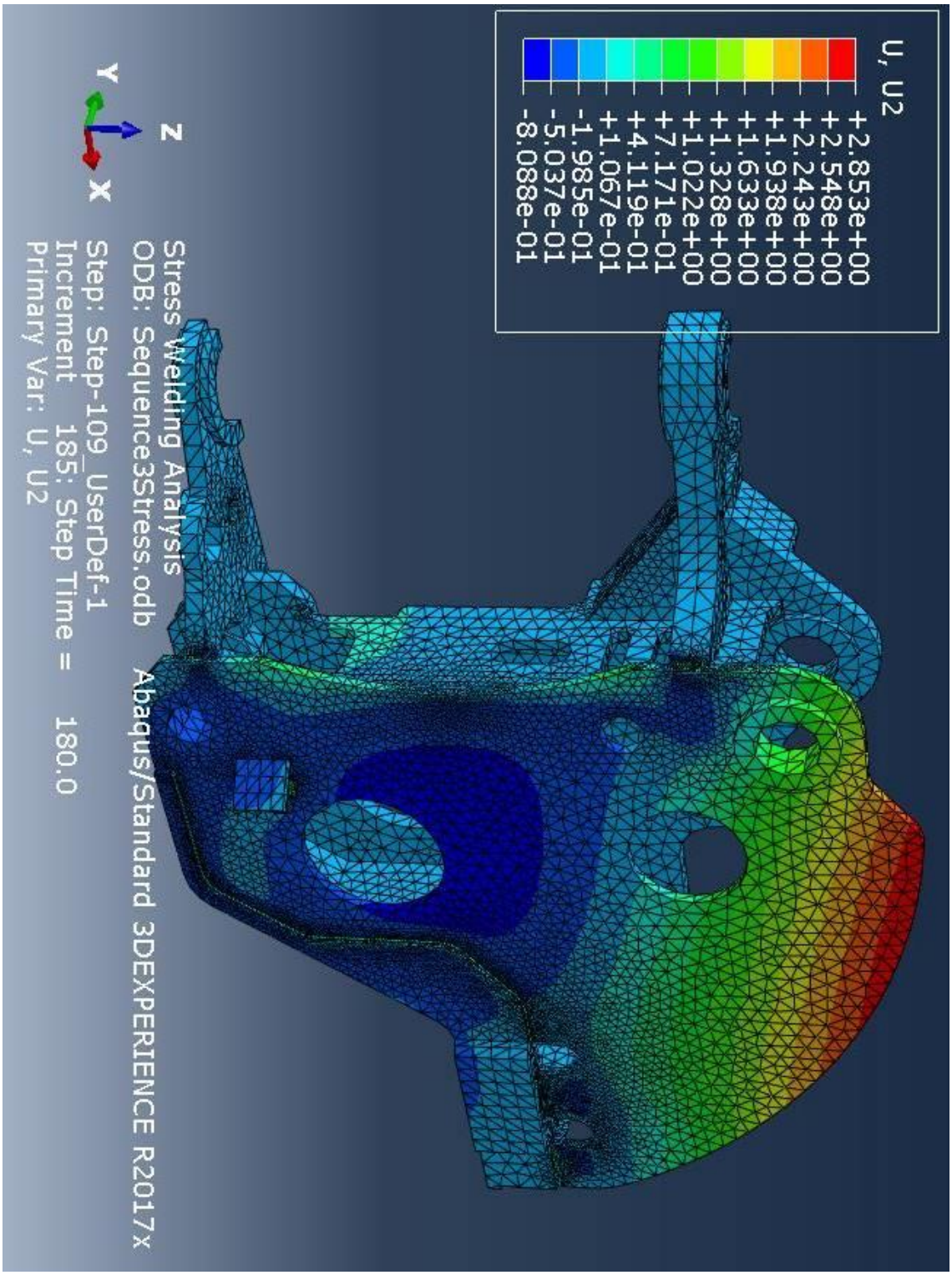

Appendix IX

Nodal displacement of selected nodes during welding with welding sequence 4

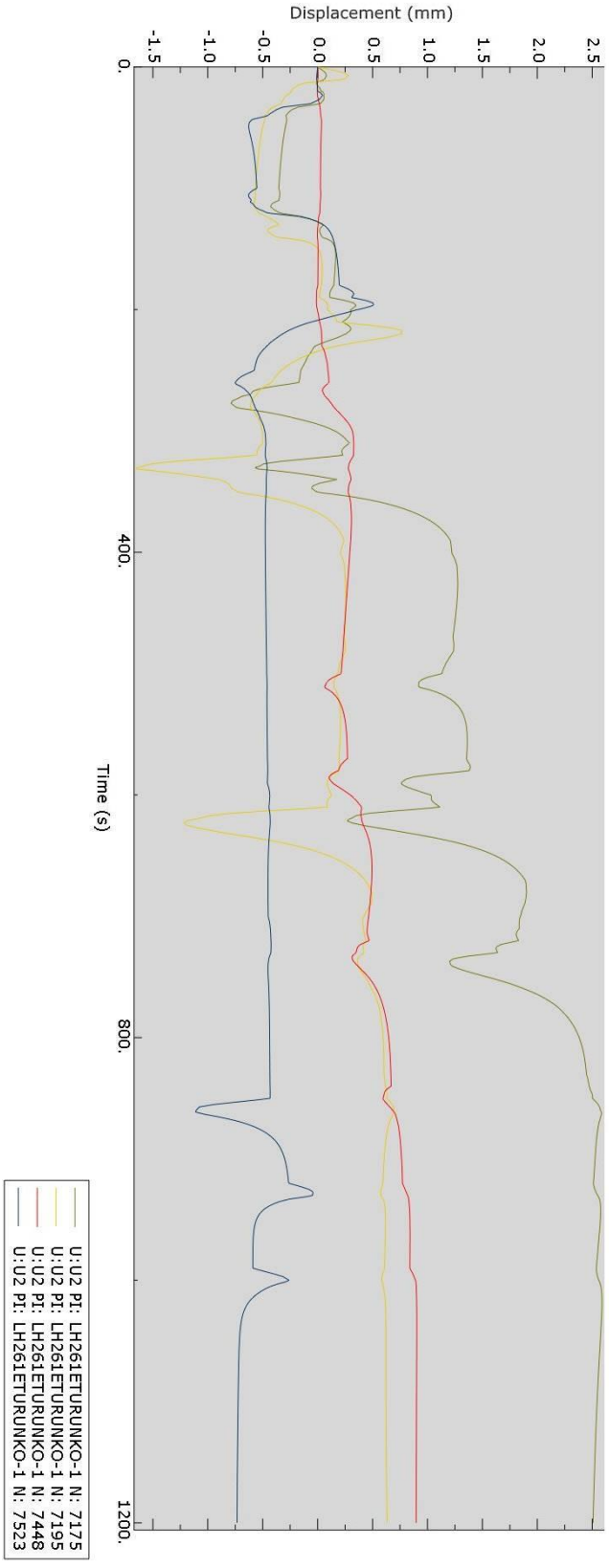

Appendix X

Final welding deformations of welding sequence 4

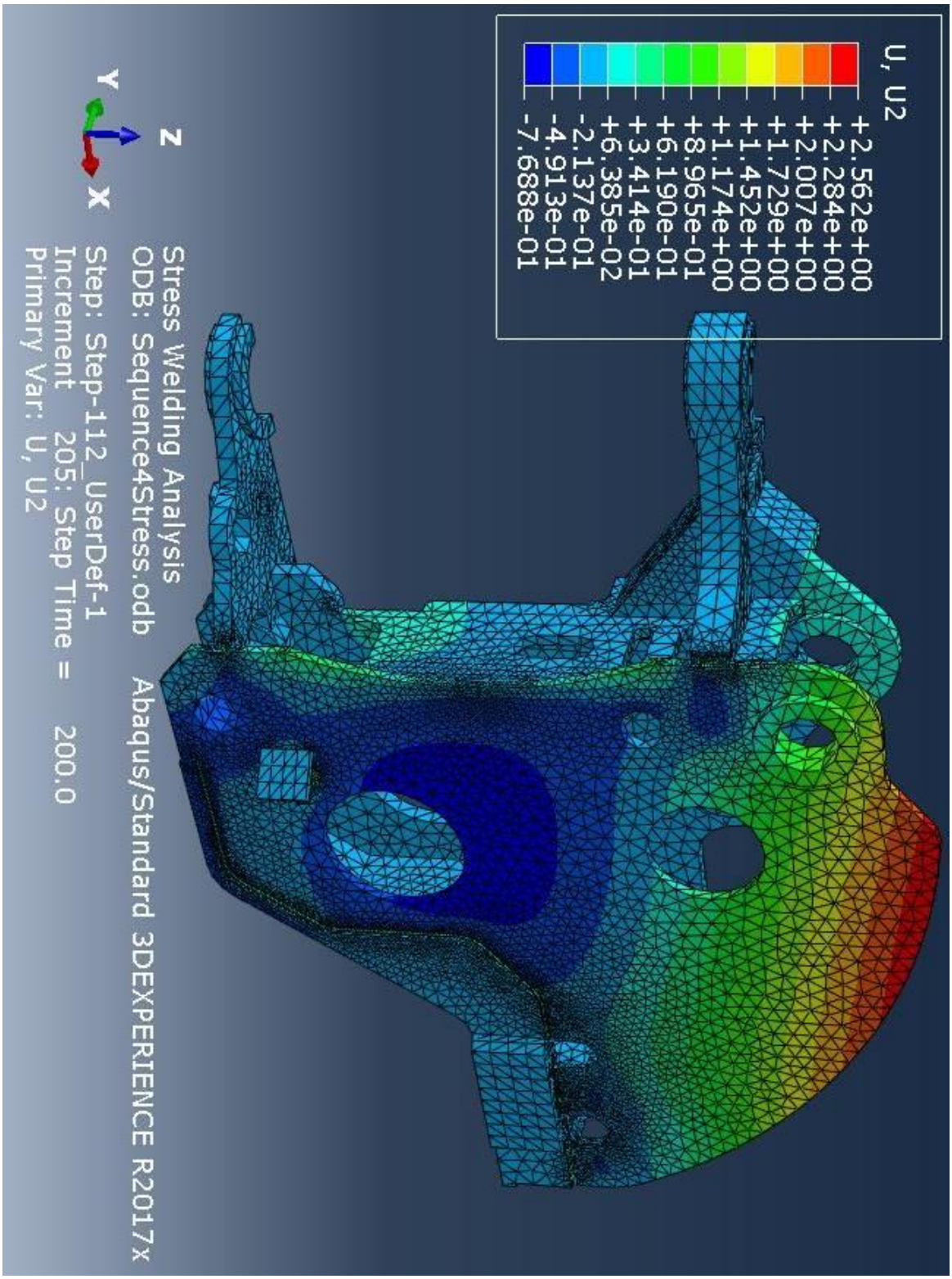

Appendix XI

Nodal displacement of selected nodes during welding with welding sequence 5

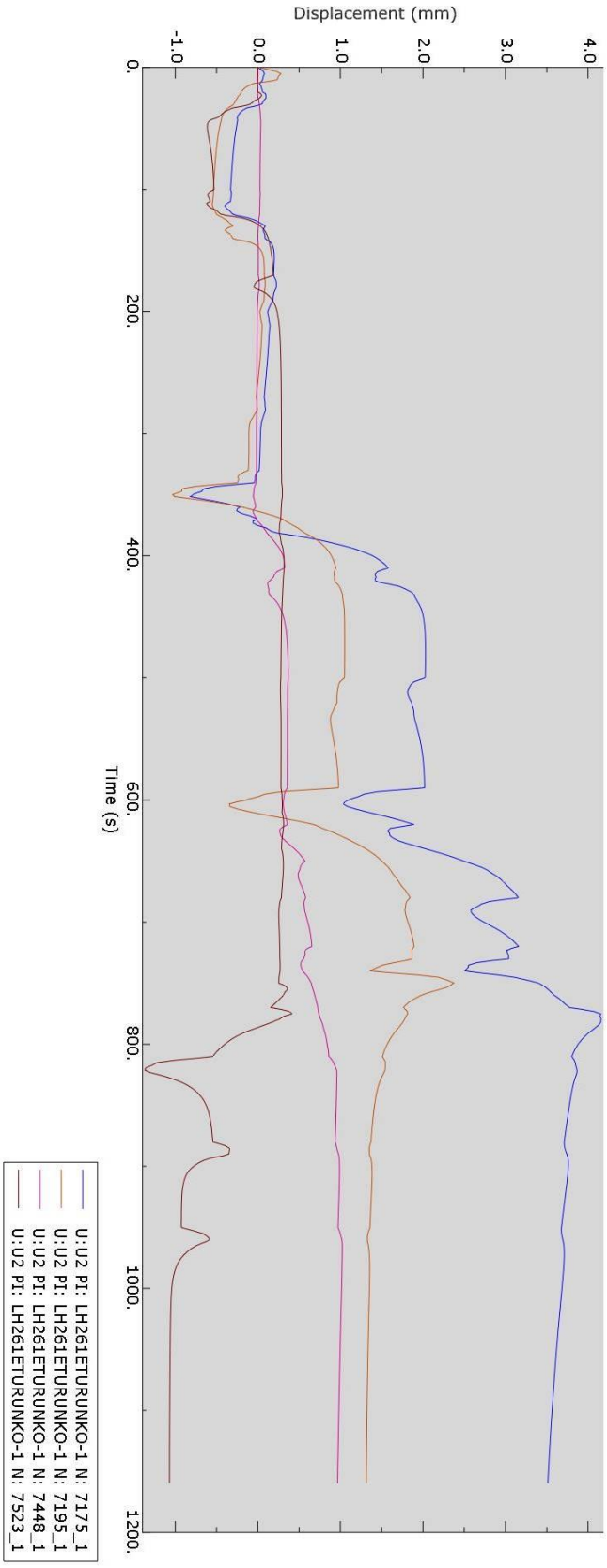

Final welding deformations of welding sequence 5

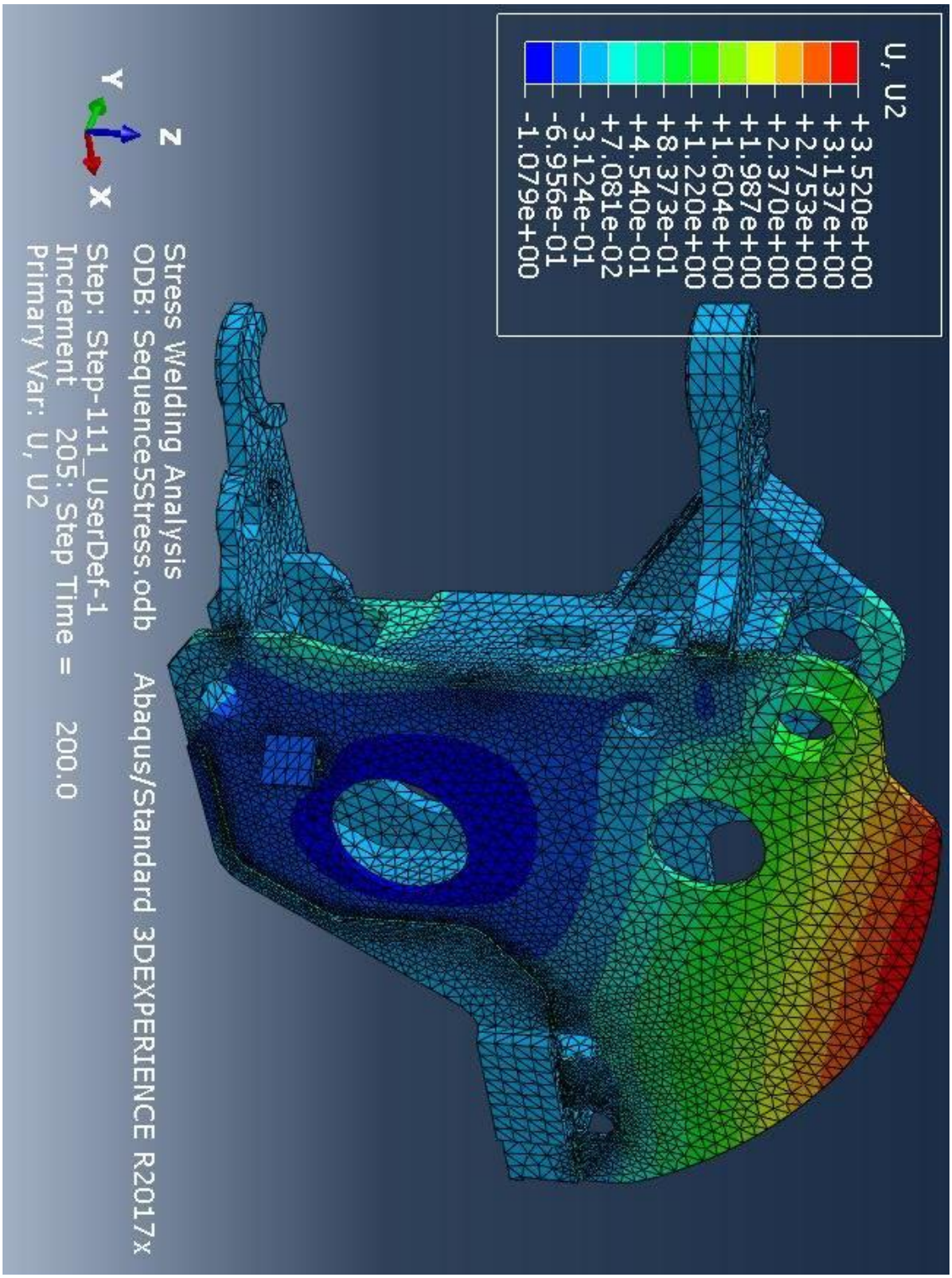

Appendix XIII

Nodal displacement of selected nodes during welding with welding sequence 6

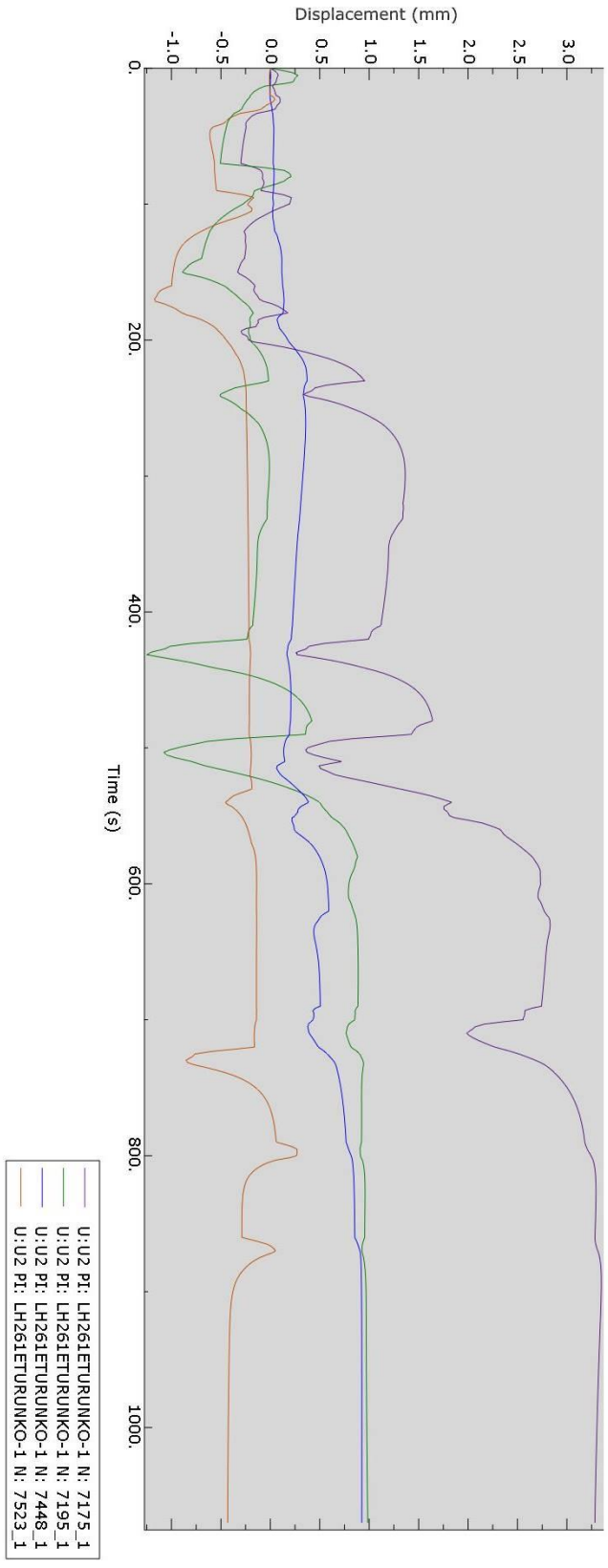

Appendix XIV

Final welding deformations of welding sequence 6

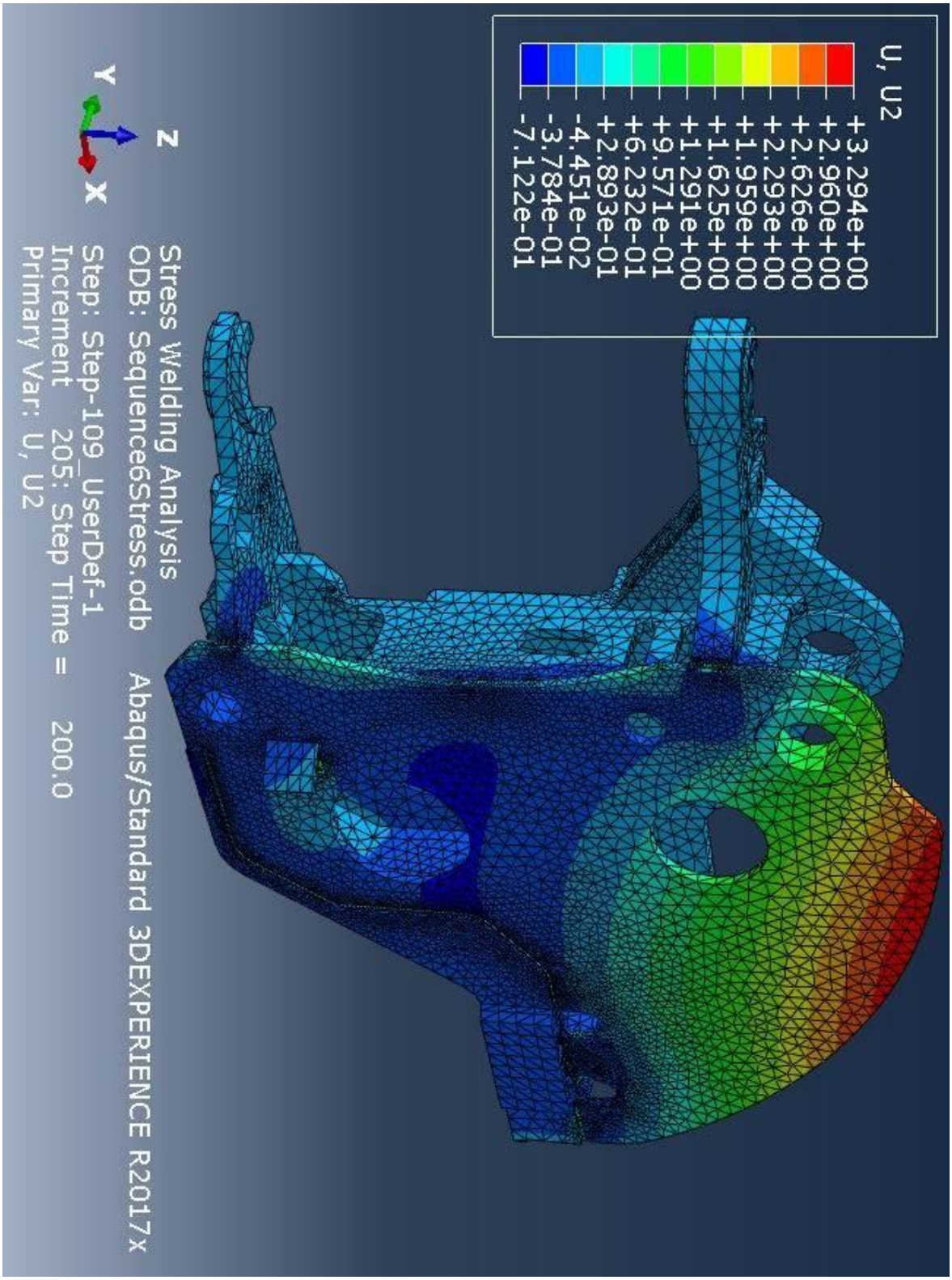

Appendix XV

Nodal displacement of selected nodes during welding with welding sequence 7

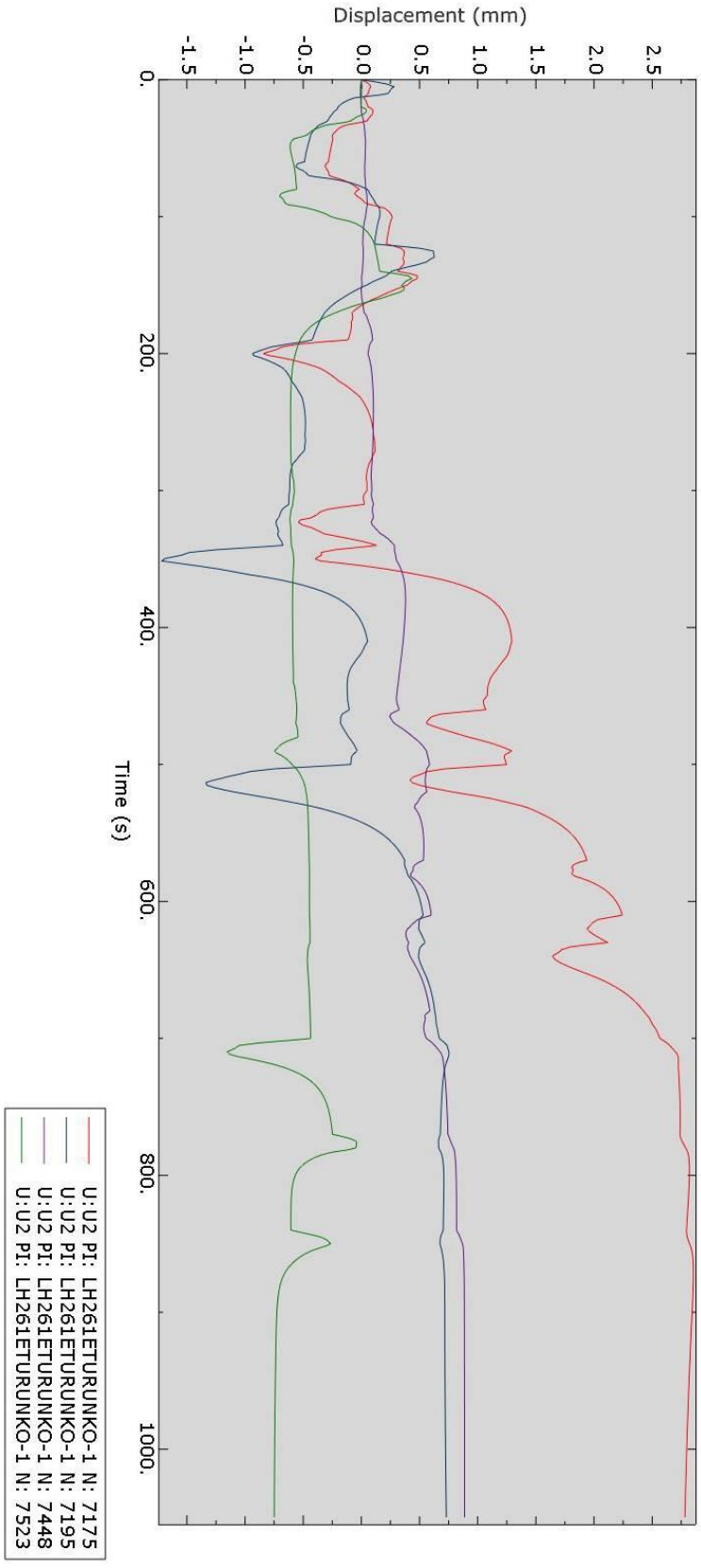

Final welding deformations of welding sequence 7

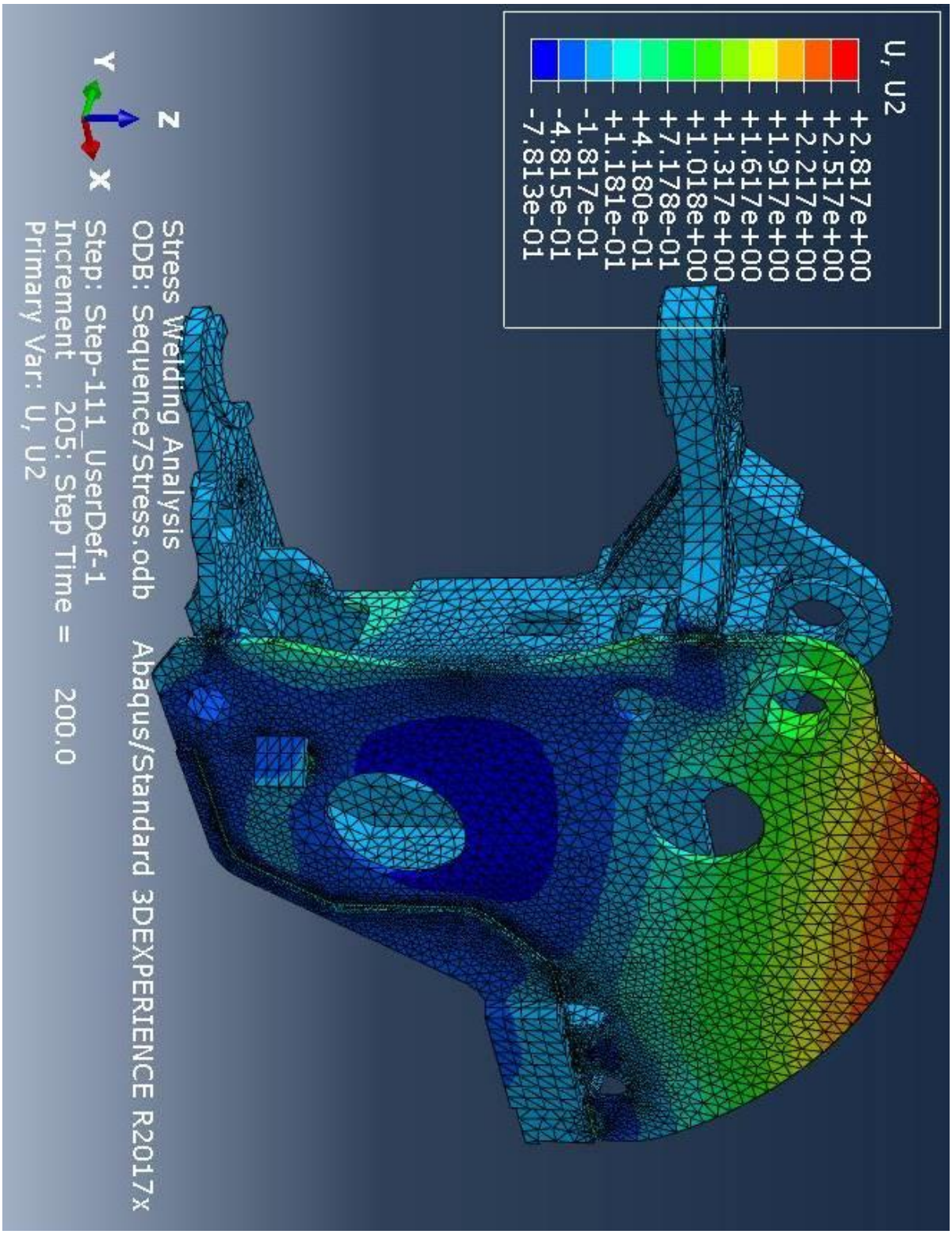

Appendix XVII

Nodal displacement of selected nodes during welding with welding sequence 8

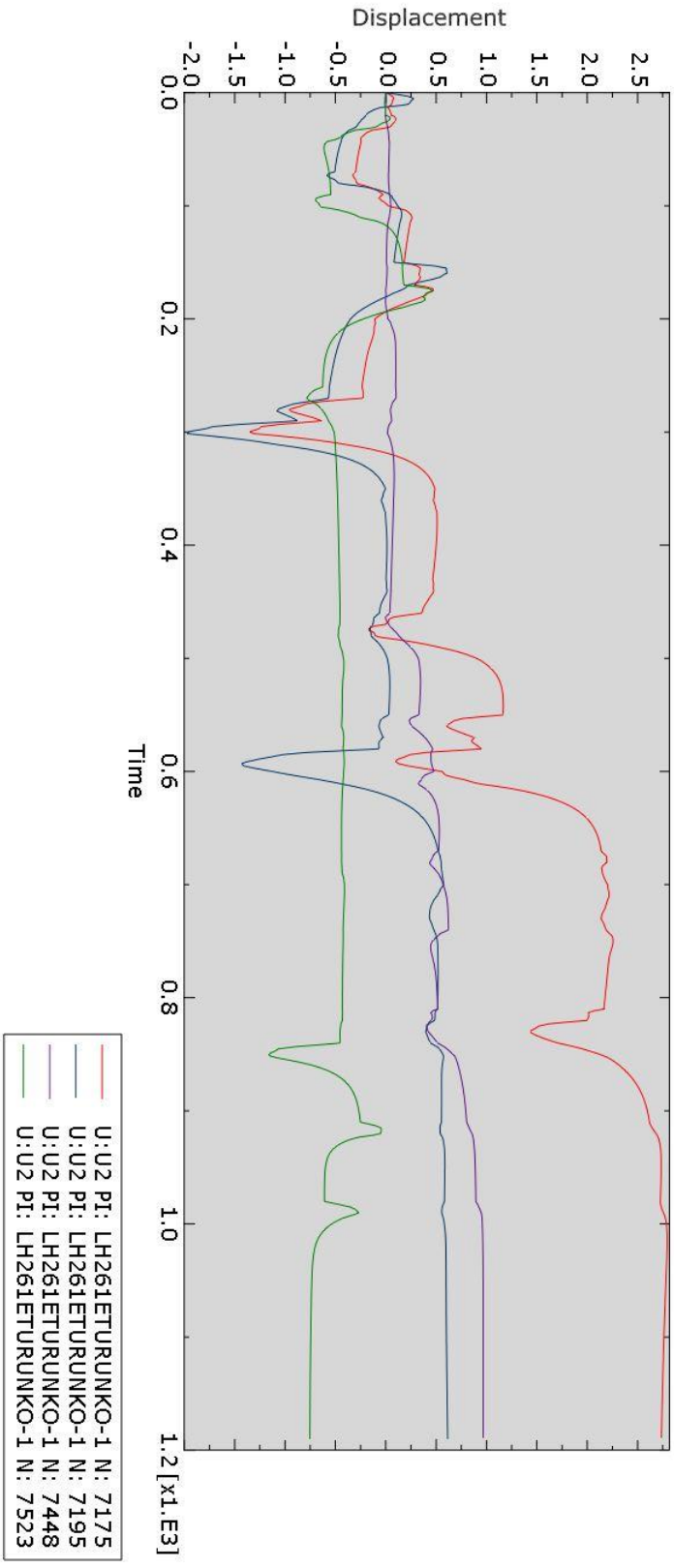

Final welding deformations of welding sequence 8

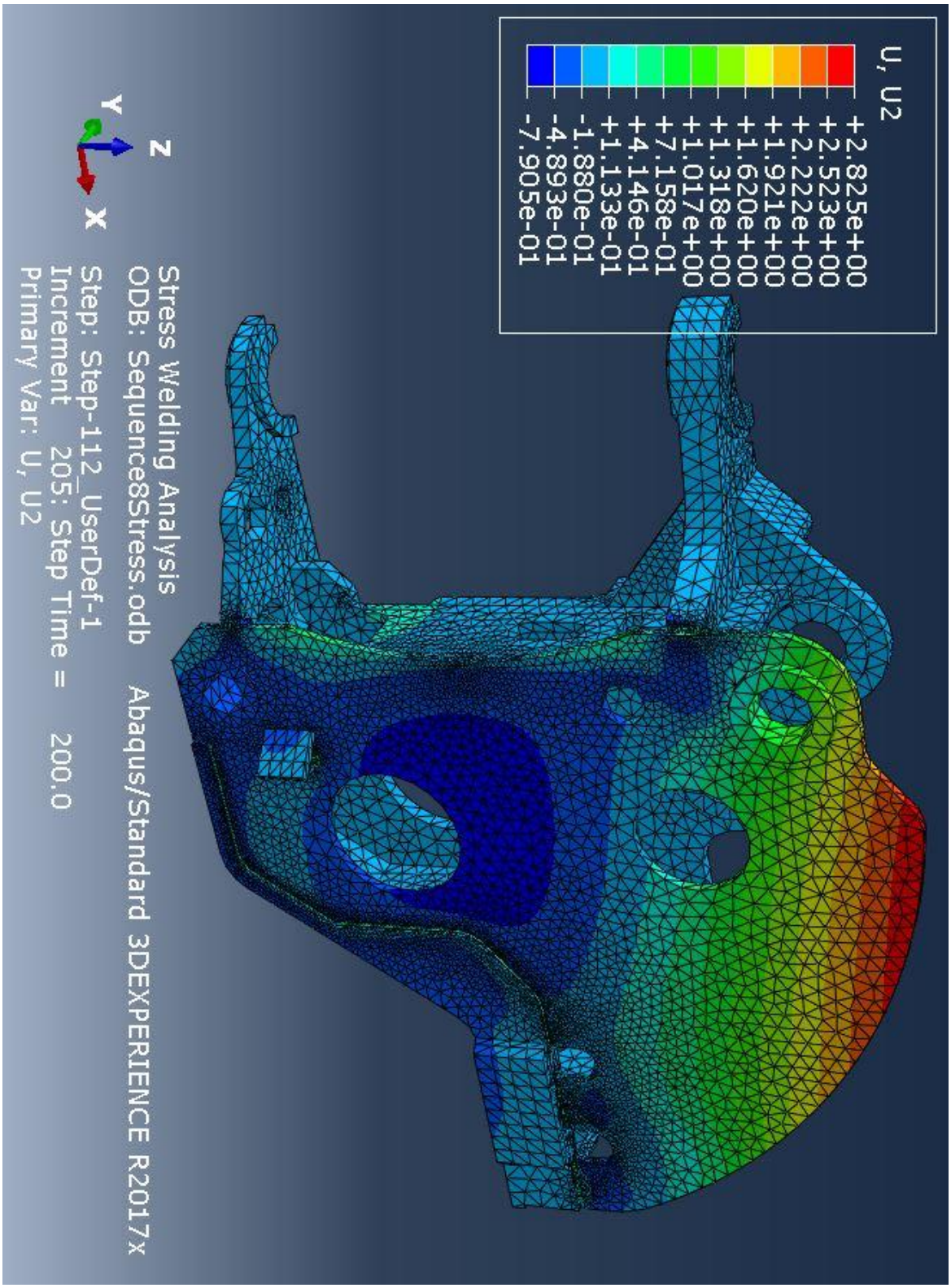

Appendix XIX

Nodal displacement of selected nodes during welding with welding sequence 9

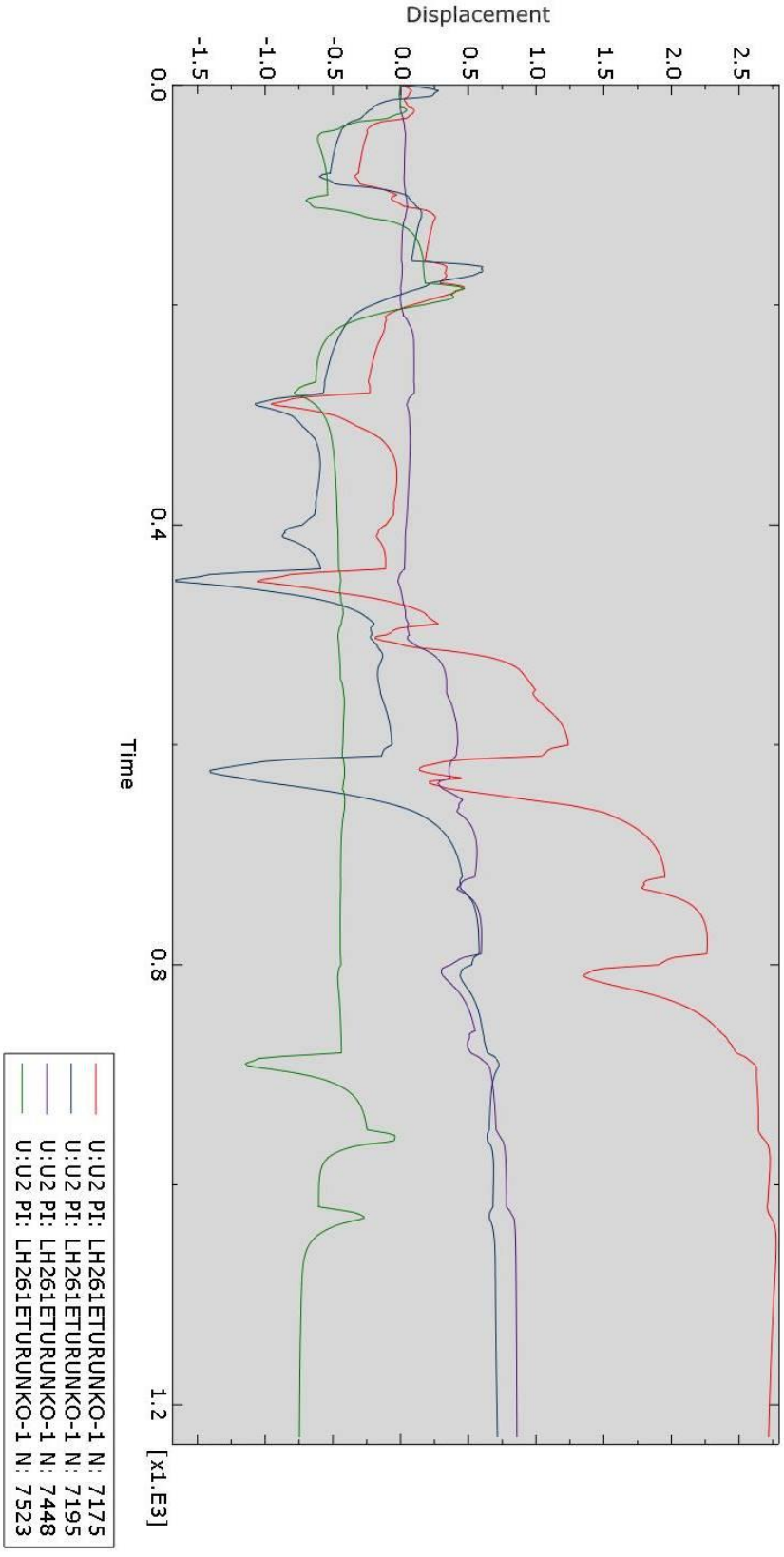

Appendix XX

Final welding deformations of welding sequence 9